Climate variability and change of Mediterranean-type climates

Richard Seager*,

Lamont Doherty Earth Observatory of Columbia University, Palisades, New York

Timothy J. Osborn

Climatic Research Unit, University of East Anglia, Norwich, United Kingdom

Yochanan Kushnir

Lamont Doherty Earth Observatory of Columbia University, Palisades, New York

Isla R. Simpson ,

Climate and Global Dynamics Laboratory, National Center for Atmospheric Research, Boulder, Colorado

Jennifer Nakamura and Haibo Liu ,

Lamont Doherty Earth Observatory of Columbia University, Palisades, New York

* *Corresponding author address:* Richard Seager, Lamont Doherty Earth Observatory of Columbia University, 61 Route 9W., Palisades, NY 10964. Email: seager@ldeo.columbia.edu

Submitted to *J. Climate* July 2018, revised November 2018, January 2019, LDEO Contribution Number xxxx.

ABSTRACT

Mediterranean-type climates are defined by temperate, wet winters and hot or warm dry summers and exist at the western edges of five continents in locations determined by the geography of winter storm tracks and summer subtropical anticyclones. The climatology, variability and long term changes in winter precipitation in Mediterranean-type climates, and the mechanisms for model-projected near-term future change, are analyzed. Despite commonalities in terms of location in the context of planetary scale dynamics, the causes of variability are distinct across the regions. Internal atmospheric variability is the dominant source of winter precipitation variability in all Mediterranean-type climate regions, but only in the Mediterranean is this clearly related to annular mode variability. Ocean forcing of variability is a notable influence only for California and Chile. As a consequence, potential predictability of winter precipitation variability in the regions is low. In all regions, the trend in winter precipitation since 1901 is similar to that which arises as a response to changes in external forcing in the models participating in the Coupled Model Intercomparison Project Five. All Mediterranean-type climate regions, except in North America, have dried and the models project further drying over coming decades. In the northern hemisphere, dynamical processes are responsible: development of a winter ridge over the Mediterranean that suppresses precipitation and of a trough west of the North American west coast that shifts the Pacific stormtrack equatorward. In the southern hemisphere, mixed dynamic-thermodynamic changes are important that place a minimum in vertically integrated water vapor change at the coast and enhance zonal dry advection into Mediterranean-type climate regions inland.

1. Introduction

Mediterranean-type climates are defined by temperate, wet winters and warm or hot dry summers. The definition originates in the Mediterranean region itself. Here winter storms bring precipitation but the subtropical location ensures cold temperatures rarely occur and the precipitation is generally rain except at high elevations. The summers are dry, apart from localized regions of convection over land, and the subtropical location and clear skies under descending air allow for high temperatures. The dynamical origins of the Mediterranean climate are, in winter, its location at the poleward edge of the winter Hadley Cell and equatorward flank of the North Atlantic storm track and, in summer, its location under a vast area of subsidence extending from the North Atlantic subtropical high, across the Mediterranean and into east Asia and encompassing North Africa as well.

Because of the location of the Mediterranean climate and its generation in terms of planetary scale dynamics, it is not surprising that there are four other regions of the world with Mediterranean-type climates. These are the west coast of North America from northern Mexico to Washington State, central Chile, the far southwest tip of southern Africa and southwest Australia. All these regions have the same winter-dominated precipitation regime, temperate winter climates and hot or warm, dry summers. The climatological similarity of the world's Mediterranean-type climate regions (MCRs) translates into similar natural vegetation with sparse woodlands, grasses and shrubs that have been converted into similar agricultural uses for growing vines (primarily for wine), fruits, olives, wheat and nuts (di Castri and Mooney 1973), the bases of the so-called Mediterranean diet with its associated health benefits (Baich-Faig et al. 2011).

All of the MCRs lie in the subtropics to mid-latitudes and on the western edge of continents. This location ensures a mild, maritime climate in winter with precipitation from storms in the extratropical storm tracks and, in the summer, warm to hot, dry summers under the influence of the eastern flanks of subtropical highs (Rodwell and Hoskins 2001; Seager et al. 2003b). The Mediterranean region itself is actually unique in that winter precipitation occurs primarily within the Mediterranean storm track (Trigo et al. 1999; Campins et al. 2011; Lionello et al. 2006; Flocas et al. 2010), which is distinct from the North Atlantic

storm track, and the summer subsidence is east of the North Atlantic subtropical high and more related to a forced response to Asian monsoon heating (Rodwell and Hoskins 1996, 2001; Simpson et al. 2015). Only the climates of Portugal and Morocco are strictly analogous in climate dynamical context to the four other Mediterranean-type climates.

All MCRs are overall semi-arid as a result of the highly seasonal precipitation and long dry summers and all struggle with water resources at the best of times. Lying between the more arid subtropics and the more humid extratropics they are locations of impactful climate variability and are highly vulnerable to intense and protracted droughts (e.g. Hurrell (1995); Smith et al. (2000); Risbey et al. (2009); Seager et al. (2014a); Cook et al. (2016); Garreaud et al. (2018)). Fire is a hazard common to Mediterranean-type climates too (Bowman et al. 2017). In recent years California has experienced withering droughts (Seager et al. 2014a; Williams et al. 2015) and fires, Chile has also experienced drought and fire (Garreaud et al. 2018), southwest Africa (around Cape Town) is enduring a severe drought (Wolski 2018; Simpkins 2018) and the Mediterranean and southwest Australia have experienced persistent dry conditions in recent decades (Allan and Haylock 1993; Kelley et al. 2011; Hoerling et al. 2012; Delworth and Zeng 2014). In addition, climate change caused by rising greenhouse gases is expected to reduce precipitation in all MCRs other than California (Polade et al. 2017) and warming will increase drought risk (Cook et al. 2014).

Given their same similar climates arising from comparable geographical locations with reference to continental geography and planetary scale circulation, it might be expected that the causes and character of climate variability and change would also be similar across the MCRs. There is an extensive literature addressing climate variability and change for the Mediterranean, California and, to some extent, Chile and somewhat less for southwest Africa and southwest Australia. However, while Polade et al. (2017) address climate change across the MCRs, to our knowledge there has yet to be a study that compares and contrasts both variability and change across the Mediterranean-type climates and places this within a mechanistic climate dynamics framework to achieve basic understanding. In this regard the similarities and differences will be informative as to the underlying processes influencing these climate regions. While all MCRs face similar climate problems, are the climate processes generating the variability and change the same or different?

In this paper we will address the following issues.

i. How similar are the climatology and variability of precipitation and temperature across the MCRs?

ii. What atmospheric circulation phenomena drive interannual variability of winter precipitation of the MCRs? What is the relative role of ocean (sea surface temperature, SST) forcing compared to internal atmospheric variability?

iii. What are the trends in winter precipitation over the past century in the MCRs? Are they consistent with expectations, based on climate models, of change due to human-induced climate change?

iv. What are the dynamical and thermodynamical mechanisms that models project will cause declines in winter precipitation in all MCRs other than California?

v. What are the common processes that lead to similar variability and change across MCRs and what are the zonally and hemispherically asymmetric processes that lead to differences across MCRs?

We begin by describing the data and then present a series of observational analyses and simulations with SST-forced models to examine variability. We will then examine simulations from the Coupled Model Intercomparison Project Five (CMIP5) to diagnose projections of radiatively-forced change and determine the mechanisms responsible. A discussion of the commonalities and differences between MCRs from a climate dynamics perspective will follow and then we will offer conclusions.

2. Mediterranean-type climate definition and observational data and model simulations used

a. Mediterranean-type climate type definition

Our definition of MCRs follows the Köppen climate classification which divides climates with 1), winters that are temperate and the season of maximum precipitation and 2), dry

summers, into two types: *Csa* hot summers and *Csb* warm summers. The categorization is that of Leemans and Cramer (1991) and is provided with details at `http://iridl.ldeo.columbia.edu/SOURCES/.UN/.FAO/.NRMED/.SD/.Climate/.dataset_documentation.html#anchor2`. The MCRs are shown on Figure 1. The Mediterranean, California and southwest Australia are dominated by the *Csa* hot summer type, and Chile and southwest southern Africa by the *Csb* warm type. Note that, according to the Koppen climate classification, the Pacific Northwest of North America is an MCR. Since, for example, Seattle is not commonly considered to have an MCR (but does have a climate similar to central Chile) we have broken the west coast of North America into the Pacific Northwest and the more commonly considered MCR of California. We also ignore the warm summer MCR in southeast Australia because of its somewhat different location in the context of planetary scale circulations. We recognize that we are adopting a broad brush climatology-inspired definition of MCR. For a more nuanced and detailed description of MCRs see Aschmann (1973). To create climate quantities within the MCRs we use shapefiles available from the International Research Institute for Climate and Society corresponding to the *Csa* and *Csb* locations in Figure 1. The red boxes in Figure 1 are there only to draw attention to the MCR regions that are depicted by the orange and burgundy shading within the boxes. Climate data were averaged over these shaded MCR regions within the boxes. The MCRs are notably different in size with southwest southern Africa the smallest and the Mediterranean the largest.

b. Observational data

For precipitation and temperature observations over land we use the latest data set from the University of East Anglia Climatic Research Unit CRU TS3.25 which provides data on a 0.5° grid at monthly resolution from 1901 to 2016 (Harris et al. 2014) accessed from `http://dx.doi.org/10.5285/c311c7948e8a47b299f8f9c7ae6cb9af`. For SST and 200hPa heights we use data from the National Centers for Environmental Prediction-National Center for Atmospheric Research (NCEP-NCAR) Reanalysis (Kalnay et al. 1996; Kistler et al. 2001) for 1949 to 2016 accessed from `https://iridl.ldeo.columbia.edu/SOURCES/.NOAA/.NCEP-NCAR/.CDAS-1/`. To assess if data limitation in the southern hemisphere prior

to the satellite era influences the results we also conducted the analyses for 1979 to 2016 and found very similar results to those for 1949 to 2016 and hence just show results for the longer period. In addition we analyzed observed precipitation data from the Global Precipitation Climatology Center (GPCC) at half degree resolution covering 1901 to 2013 (Schneider et al. 2011), accessed from `http://iridl.ldeo.columbia.edu/SOURCES/.WCRP/.GCOS/.GPCC/.FDP/.version7/.0p5/` and for the U.S. from the PRISM group at Oregon State University (Daly et al. 2008) (available at `www.prism.oregonstate.edu`, accessed 6/21/18).

c. SST-forced atmosphere model simulations

To examine SST-forced variability we use a 16 member ensemble of simulations of the NCAR Community Atmosphere Model 5.3 (see `http://www.cesm.ucar.edu/models/cesm1.2/cam/docs/ug5_3/ug.html#idm218596792640`, CAM5.3) forced by Hadley Centre SST data HadISST1 (Rayner et al. 2003). Atmospheric trace gas contents were held fixed (mixing ratios are $CO_2 = 3.55 \times 10^{-4}, CH_4 = 1.71 \times 10^{-6}, N_2O = 0.311 \times 10^{-6}, F11 = 0.28 \times 10^{-9}, F12 = 0.503 \times 10^{-9}$). The 16 members are begun from different initial conditions on January 1 1856 such that the unforced variability in each member is uncorrelated with that in each other member. We analyze the mean across the ensemble members which isolates the SST-forced component of the atmosphere simulations common to all members. The simulations were generated at Lamont and run at T42 spectral resolution with 30 vertical hybrid-sigma levels.

d. Radiatively-forced model simulations

To examine climate change caused by external forcing, such as changes in the trace gas content of the atmosphere due to human activity, we use models from the Coupled Model Intercomparison Project Five (CMIP5, Taylor et al. (2012)). Since we conduct an analysis of the contributing terms to changes in precipitation we use all the models that make available all the data needed for evaluation of the moisture budget with sufficient vertical resolution to perform vertical integrals and at 6 hourly time intervals to allow evaluation of moisture

transports by transient eddies. These are the same 22 models as in Seager et al. (2014c). To create a multimodel ensemble mean we first evaluate the mean of ensemble members for each model using runs continuous between historical and future projections and then average across models. Thus each model receives equal weight in the multimodel ensemble mean despite different ensemble sizes for models. For the 1901 to 2005 period we use the historical all-forcings simulations and for 2006 to 2040 we use the RCP8.5 emissions scenario projections. All model data are regridded to a common $1^\circ \times 1^\circ$ grid. The list of models, their origin and some details are provided in Table 1.

3. Climatology and variability of climate for Mediterranean-type climates

a. Climatology

To understand the large-scale dynamical context of MCRs we plot in Figure 2, for the November to February and May to August seasons, the land precipitation and sub-monthly 200hPa meridional velocity variance, a common measure of the extratropical storm track (see, for example, Berberry and Vera (1996); Chang et al. (2002)), and sea level pressure. In winter, the location of the MCRs poleward of arid subtropical regions with, in North America and Europe, more humid regions on their poleward side, is clear and arises from their positioning in, or on the equatorward flank of, the mid-latitude storm track. The storm track provides the winter precipitation. In the summer, the mid-latitude storm track is weaker and further poleward and each MCR is on the eastern flank of the subtropical anticyclones and hence under equatorward flowing, descending air (Rodwell and Hoskins 2001; Seager et al. 2003a). This provides for the warm or hot and dry summers. The Mediterranean itself is under a ridge expanding eastward from the North Atlantic subtropical high that is likely connected to Asian monsoon-induced subsidence (Rodwell and Hoskins 1996, 2001; Simpson et al. 2015). The commonality of the MCRs in terms of the large-scale dynamics context is clear and establishes the broad similarity in these climates on five continents.

Figure 3 shows the climatological seasonal cycle of precipitation and temperature for the

six MCRs. The six MCRs have remarkably similar seasonal cycles: maximum precipitation in December-January (June-July) and minimum precipitation in July-August (December-January) in the northern (southern) hemisphere. The temperature seasonal cycles are similarly comparable: minimum temperature in December-January (June-August) and maximum temperature in July-August (December-February) in the northern (southern) hemisphere. Absolute precipitation and temperature do, however, differ across MCRs. In order from wettest to driest precipitation maxima, the MCRs are: Pacific Northwest, California, Chile, and then Mediterranean, southwest southern Africa and southwest Australia as a group. In order from warmest to coolest summer temperature maxima, the MCRs are: Mediterannean, southwest Australia, southwest southern Africa, California, Pacific Northwest, Chile. Figure 1 also shows the annual mean precipitation which makes clear the variation in seasonal maximum precipitation is reflected in the variation of overall aridity with the Pacific coast MCRs being less arid than the Mediterranean, southern Africa and Australian MCRs.

Figure 3 also shows box and whiskers plots of the median, 25th and 75th percentile, the $\pm 2.7\sigma$ range and outliers (beyond $\pm 2.7\sigma$ for a normal distribution) for the temporal distribution of area mean precipitation for each month in each MCR. Again there is much similarity across MCRs. The summer dry season is a time of very little precipitation variability while the winter wet season has substantial variability. The size of the 25th to 75th percentile range typically equals a quarter to a third of the value of the monthly mean precipitation but the full range of monthly precipitation (excluding outliers) varies from next to no precipitation to twice the normal. The three northern hemisphere MCRs have maximum temperature variability during the wet season but in the southern hemisphere temperature variability is more evenly spread through the year. Although not investigated here, we suspect this inter-hemispheric difference is due to the large area of continents in the northern hemisphere that get cold in winter causing large land-sea and meridional temperature contrasts that circulation variability can translate into large amplitude temperature variability (Schneider et al. 2015).

b. Interannual variability of winter precipitation

1) Observed relations

The seasonal cycles clearly suggest that variability of a four month winter season mean precipitation will be the dominant feature of interannual hydroclimate variability in MCRs with likely impacts on water resources, hydrology and ecosystems. For the northern hemisphere we define November through February, and for the southern hemisphere we define May through August, as four month averaged periods to analyze and for convenience refer to these as the winter seasons. It is recognized that such temporal averaging is rarely ideal since the phenomena that influence variability within the season and the seasonal cycle itself occur within a time continuum. Given their subtropical locations and exposure to winter storm tracks that can be displaced by tropically-forced teleconnections (e.g. Trenberth et al. (1998); Seager et al. (2003a)), it might be expected that each of the MCRs would be influenced to some degree by the dominant source of SST-forced interannual variability, the El Niño-Southern Oscillation (ENSO). Also, given their latitude, it might be expected that MCRs will be at the equatorward flank of variability induced by the northern and southern annular modes. In addition, other modes of SST-forced and internal variability could be important.

In Figure 4 we show the regression of winter mean 200hPa geopotential heights and SST on concurrent winter mean precipitation anomalies in the MCRs for the 1949 to 2016 period covered by the NCEP-NCAR Reanalysis. To remove long term climate change, to be considered separately below, these analyses are conducted on data that have been linearly detrended. Despite the above expectation, only California and Chile show a connection of winter wetness to ENSO and only weakly so. The association is in the sense of El Niño (La Niña) winters tend to be wet (dry) but we know based on prior work (Seager et al. 2015; Jong et al. 2016) that the association for California is largely restricted to the El Niño-wet side.

Not only is the ENSO influence restricted to those MCRs that border the eastern Pacific Ocean, but this appears the only ocean influence on MCR winter precipitation variability. For the Pacific northwest, Mediterranean, southwest southern Africa and southwest Australia the

results show no regions with statistically significant SST anomalies that appear to be forcing precipitation variability. For the Pacific northwest the SST anomalies that do appear are consistent with forcing from the atmosphere in the form of cold/dry (warm/moist) advection generating enhanced (reduced) ocean to atmosphere surface heat flux and cool (warm) SST anomalies. The cool waters west of southwest Australia are also consistent with cooling due to enhanced westerlies. The height anomalies associated with southwest Southern Africa winter precipitation variability are similar to those previously noted by Reason et al. (2002).

The signal of the northern annular mode shows up clearly in relation to Mediterranean winter precipitation variability. Wet winters go along with a negative northern annular mode that would also be a negative North Atlantic Oscillation (NAO) with anomalous high heights over the subpolar North Atlantic and northern high latitudes and negative heights over the subtropical Atlantic and subtropical northern latitudes. The height anomalies are positioned so that during wet winters the Mediterranean region experiences enhanced westerly flow. Although the annular mode anomalies are hemispheric in scale, the dominant mode influencing winter precipitation variability in the Pacific Northwest is instead a North Pacific to North Atlantic wave train that places, during wet winters, strong westerlies over the region and which appears to arise from internal atmospheric variability. Any influence of the southern annular mode is not leading for any of the three southern hemisphere MCRs. Chile instead reflects an ENSO influence, and both southwest southern Africa and southwest Australia tend to have wet (dry) winters when local westerlies are strong (weak) with only southwest Australia having some hint of being related to annular mode of variability (and perhaps more to an Australian regional version of the Antarctic Oscillation as in Meneghini et al. (2007)).

These results are consistent with, or not inconsistent with, prior work on SST relations to precipitation variability in MCRs. Seager et al. (2015) review work on California winter precipitation variability and show that there is a weak correspondence of El Niño events to wet winters but no association between La Niña and dry winters. Garreaud et al. (2018) show an ENSO association to winter precipitation variability in Chile. This is consistent with the hemispherically symmetric aspects of ENSO-driven climate variability (Seager et al. 2003a) with the anomalies in Chile occurring in the northern summer (southern winter) before peak

ENSO events and the impact on California in the following northern winter. We have shown an association between the NAO and Mediterranean winter precipitation which has been long known (Hurrell 1995). Recently it has been claimed that the winter NAO is significantly driven by tropical SST variations (Scaife et al. 2014) but those SST-forced variations do not appear in our analysis due to the dominant internal atmospheric origin of NAO variability. For southwest southern Africa an apparent connection of ENSO to precipitation variability occurs in the dry season (Rowell 2013) and, while Philippon et al. (1985) claimed an ENSO connection to wet season precipitation variability during 1979 to 1999 for the wider southwest, this is actually weak in the MCR (see their Figure 5). The association of wet and dry winters in southwest Australia with anomalous westerlies and easterlies was noted by Allan and Haylock (1993) and Smith et al. (2000). An association of wet (dry) with La Niña (El Niño) is obscured in this analysis since it does not reach statistical significance which is consistent with the ENSO teleconnection to Australia being focused in the east of the continent and only weakly influencing the Australian MCR (Risbey et al. 2009). That the ENSO relation to the southern hemisphere MCRs is weak is consistent with O'Kane et al. (2017) who emphasize the importance of internal mid-latitude waveguide dynamics to circulation variability across the southern hemisphere.

2) Model-based analysis of SST-forced precipitation variability in MCRs

Based on the results in the prior subsection we would not expect a high level of agreement between the observed time series of winter precipitation in MCRs and those simulated by SST-forced models. This is because the observational analysis does not identify a role for SST forcing other than in California and Chile where it is still, nonetheless, quite weak. Figure 5 shows the observed and model ensemble mean time histories of winter precipitation and temperature for each MCR as well as, with shading, the spread across the model ensemble. In California, Chile and southwest Australia the ensemble mean precipitation time series is correlated with the observed history at the 5% statistical significance level (according to a two-sided t-test) but with correlation coefficients of 0.17, 0.42 and 0.19 respectively. Hence Chile is the only MCR where SST-forcing appears to explain more than 10% of the total

variance of winter precipitation.

The SST-forced climate model experiments allow further interrogation of the role for SST-forcing. The ensemble mean of the simulations closely identifies the SST-forced component common to each ensemble member. Figure 6 is as for Figure 4 but computed on the ensemble mean of the SST-forced simulations with CAM5.3. Here we use only the 1949 to 2016 period of the model simulations to match the NCEP-NCAR period analyzed above. Here we uncover the maximum potential for the oceans to drive winter precipitation variability in the MCRs. For the Pacific northwest, La Niña conditions have a weak relation to wet winters. For both California and Chile there is a clear association in the SST-forced signal between El Niño and wet winters. The fact that this is less clear in the observational analysis is almost certainly due to the strength of internal atmosphere variability and its influence on precipitation in these regions. For the Mediterranean too, an ENSO influence is apparent consistent with Scaife et al. (2014), while Pozo-Vasquez et al. (2005, 2001) show the relation is primarily La Niñas favoring a positive NAO and dry conditions across most of the Mediterranean. The ENSO-Mediterranean precipitation teleconnection may also vary over time due to the influence of other modes of variability and location of tropical Pacific SST anomalies (Lopez-Parages and Rodriguez-Fonseca 2012; Lopez-Parages et al. 2016). Significant, however, is that here we find this SST-forced precipitation signal is weak compared to that of the NAO. Since the NAO is primarily a mode of internal atmosphere variability and only weakly SST-forced, these results are consistent with the observational analysis identifying internal atmosphere (NAO) variability, not SSTs, as the leading cause of winter precipitation variability in the Mediterranean. There is essentially no SST-forced signal over southwest southern Africa and the association between wet winters in southwest Australia and La Niña is consistent with Risbey et al. (2009) in both sign and weak amplitude.

The time series of observed winter precipitation in all the MCRs (Figure 5) show strong variability and any long term trends are weak in comparison but, close inspection, shows likely drying trends in the Mediterranean, Chile, southwest southern Africa and southwest Australia, which we examine in the next section. Warming trends appear clearly in the Mediterranean, Chile, southwest southern Africa and southwest Australia. The trends are faithfully reproduced by the SST-forced model but it is also notable that the interannual

variability of surface temperature is too (numbers in parentheses show correlation coefficients for detrended time series). Further examination, not shown here, shows this to be of little interest because warm anomalies are caused by circulation anomalies that also warm the waters offshore from the MCRs. When these warm water anomalies are imposed in the model it causes a warm response in the MCRs even though the responsible circulation anomalies are not simulated, i.e. the right answer for the wrong reason.

4. Long term change in precipitation in Mediterranean-climate regions

a. Observed and modeled trends over the past century

Figure 7 shows the linear trend in land precipitation over 1901 to 2016 that was removed before conducting the analyses shown in the previous section. In both California and the Pacific Northwest the trend within the MCR is spatially variable. In contrast, there has been widespread drying across Chile, southwest Australia and the Mediterranean, except Iberia. In the very small MCR of southwest southern Africa there has also been drying. Figure 8 shows the multimodel mean trend over the same period in the CMIP5 models. This bears notable similarity to the observed trend. In the models, of the six MCRs only the west coast of North America has got wetter while the other four have dried. The spatial patterns in which the MCR precipitation change occurs are also similar between observations and model response to external forcing. In North America this is widespread wetting over the US but drying in western Mexico. In the Mediterranean region observations and models agree on drying across North Africa and around the north shores of the Mediterranean Sea. In Australia there is agreement on drying of all of southwest Australia not just the MCR. There is disagreement in South America with the models suggesting wetting south of the Chile MCR but the observations extending the drying into the humid region to the south. In Africa the models are more emphatic in drying all of southern Africa. Nonetheless, given the strength of natural variability, uncertainties in the observational data and potential model errors and biases, this comparison is suggestive that each of the MCRs is already experiencing

forced and human-induced precipitation change.

The lower panel of Figure 8 shows box and whiskers plots of the distribution of trends across the CMIP5 model ensemble. The median is plotted as the horizontal line across the box and the upper and lower limits of the box are the 25th and 75th percentiles of the distribution across models, the range is shown by the whiskers, outliers by red crosses and the mean by a black asterisk. It is striking that for the Mediterranean, Chile, southwest southern Africa and southwest Australia the model ensemble spread is predominantly drying, further indicating the robustness of this human-induced climate change signal. In this panel we also show the trends from the CRU and GPCC observational data and both show drying indicating a large degree of model-observations agreement on aridification. The model ensemble indicates wetting for California and a wet tendency for the Pacific northwest. Both are on the wet side of the observational trends (including PRISM) which are close to neutral. While much southern hemisphere climate change over recent decades has been attributed to ozone depletion that is for the summer half year when stratospheric ozone can absorb solar radiation (e.g. Polvani et al. (2011)). In the winter season, ozone depletion is unlikely to be influential (Thompson et al. 2011; Franzke et al. 2015) and the radiatively-forced changes arise instead from the increase in GHGs.

Models agree that the MCRs of the Mediterranean, Chile, southwest southern Africa and southwest Australia should be drying and the observations in these MCRs do indeed show drying. By using a bootstrapping methodology on the observed data we can assess the probability that these four MCRs would have simultaneously dried, to the degree seen in observations, through the chance sampling of interannual variability alone. All correlations of the interannual variability between these four regions are less than 0.06 and no regions have significant autocorrelation in precipitation from one year to the next except for southwest Australia where it is reduced to insignificant values when the century long trend is removed. The lack of autocorrelation of the interannual variability means it is appropriate to compare the observed trends to the distribution of trends obtained from time series constructed by randomly selecting individual years (with replacement) from the observed record. The probability of obtaining the observed magnitude of trends by chance are 9.3% for the Mediterranean, 5.2% for Chile and 26.7% for southwest southern Africa and essen-

tially zero for southwest Australia. For the regions other than southwest Australia, while individually they have not dried significantly more than expected from the sampling of interannual variability at the 5% level, the chances of obtaining a simultaneous drying of these three regions of the magnitudes observed, given their independence, is only around 0.1% i.e., $p = 0.093 \times 0.052 \times 0.267$. These statistical analyses raise confidence that the observed drying in the four MCRs where models simulate drying would not have arisen from internal climate variability alone and that external forcings have made an important contribution.

b. Model projections of near term future change in the hydrological cycle over Mediterranean-type climates and the physical causes

Here we use the CMIP5 models to determine the winter hydroclimate change they project for the coming decades and the mechanisms responsible. First in Figure 9 we show the model agreement on sign of winter precipitation change for 2021-2040 relative to 1979-2005 (the same near-term future and recent past periods used by Seager et al. (2014b,c)). The models project all MCRs except in North America to continue to dry in coming decades and this is robust (more than three quarters of models agree on the sign of the change and agree with the ensemble mean change) for all of the drying MCRs. Together with the ability of the CMIP5 models to simulate historical drying this raises confidence that the changes to be discussed are robust projections of the models.

To examine mechanisms of hydroclimate change we use a moisture budget breakdown methodology as in Seager et al. (2010, 2014b,c) using the "best-practises" methods of Seager and Henderson (2013). We divide all quantities into monthly means, represented by overbars and departures from monthly means, represented by primes with climatological monthly means denoted by double overbars. Then the vertically integrated moisture budget, written with model layer indicated by k and K the total number of levels, can be rewritten

as:

$$\Delta\overline{\overline{P}} - \Delta\overline{\overline{E}} \approx -\frac{1}{g\rho_w}\nabla\cdot\sum_{k=1}^{K}\Delta(\overline{\overline{\mathbf{u}}_k\,\overline{q}_k\overline{dp}_k}) - \frac{1}{g\rho_w}\nabla\cdot\sum_{k=1}^{K}\Delta(\overline{\overline{\mathbf{u}'_k q'_k}\,\overline{dp}_k}), \quad (1)$$

$$\approx -\frac{1}{g\rho_w}\sum_{k=1}^{K}\Delta(\overline{(\overline{\mathbf{u}}_k\cdot\nabla\overline{q}_k)\,\overline{dp}_k}) - \frac{1}{g\rho_w}\sum_{k=1}^{K}\Delta(\overline{\overline{q}_k\nabla\cdot\overline{\mathbf{u}}_k\overline{dp}_k})$$

$$-\frac{1}{g\rho_w}\nabla\cdot\sum_{k=1}^{K}\Delta(\overline{\overline{\mathbf{u}'_k q'_k}\,\overline{dp}_k}) - \frac{1}{g\rho_w}\Delta(\overline{\overline{q_s\mathbf{u}_s\cdot\nabla p_s}}). \quad (2)$$

Here $\Delta(\cdot)$ indicates change from an average over one period to an average over another period, P is precipitation, E is evaporation (taken to include transpiration), g is the acceleration due to gravity, ρ_w is the density of water, p is pressure, q is specific humidity and $\mathbf{u}$ the vector horizontal velocity. The first and second terms on the right of Eq. 1 are the moisture convergence by the mean flow and submonthly transient eddies, respectively. The approximation in Eq. 1 comes from neglecting time rate of change of moisture (which is small compared to the other terms) and ignoring terms involving dp'_k which is acceptable (see Seager and Henderson (2013))). In Eq. 2 the change in mean flow moisture convergence has been broken down into components. The first involves the change in moisture advection, i.e. flow across spatial gradients of moisture. The second involves change in moisture convergence related to the divergent flow. This is primarily influenced by mass divergence or convergence in the lower levels where moisture is concentrated. The third (the fourth term on right hand side) is a surface term that arises from bringing the divergence operator inside the vertical integral in order to enable the separation into advection and mass divergence terms.

The moisture budget change can be further decomposed into terms related to (i) changes in humidity with unchanged circulation and (ii) changes in circulation with unchanged humidity. The terms related to the moisture advection and the mass divergent flow can be approximated as:

$$-\frac{1}{g\rho_w}\sum_{k=1}^{K}\Delta(\overline{(\overline{\mathbf{u}}_k\cdot\nabla\overline{q}_k)\,\overline{dp}_k}) \approx -\frac{1}{g\rho_w}\sum_{k=1}^{K}\overline{\overline{\mathbf{u}}}_{k,20}\cdot\Delta\left(\overline{\nabla\overline{q}_k\overline{dp}_k}\right) - \frac{1}{g\rho_w}\sum_{k=1}^{K}\nabla\overline{\overline{q}}_{k,20}\cdot\Delta(\overline{\overline{\mathbf{u}}_k\overline{dp}_k}), \quad (3)$$

$$-\frac{1}{g\rho_w}\sum_{k=1}^{K}\Delta(\overline{\overline{q}_k\nabla\cdot\overline{\mathbf{u}}_k\overline{dp}_k}) \approx -\frac{1}{g\rho_w}\sum_{k=1}^{K}\Delta(\overline{\overline{q}_k\overline{dp}_k})\nabla\cdot\overline{\overline{\mathbf{u}}}_{k,20} \;-\; \frac{1}{g\rho_w}\sum_{k=1}^{K}\overline{\overline{q}}_{k,20}\Delta(\overline{\nabla\cdot\overline{\mathbf{u}}_k\overline{dp}_k}). \quad (4)$$

Further approximation comes from ignoring terms quadratic in Δ, covariances of anomalous monthly means and from using the 1979 to 2005 values for dp_k. In Eqs. 3 and 4 the first terms on the right are referred to as the 'thermodynamic terms' since they involve the changes in humidity while the circulation is fixed and the second terms are referred to as the 'mean circulation dynamics' terms since they involve the changes in the circulation while the humidity is fixed. The thermodynamic term is, however, not solely thermodynamic since the humidity field itself can change due to circulation change, not just temperature change.

The computation was carried out exactly as in Seager and Henderson (2013) to which the reader is referred to for more details. Briefly, 6-hourly data are used to compute the transient moisture fluxes and monthly mean data to compute the monthly mean moisture fluxes. In the vertical integral monthly mean pressure thicknesses are used. Derivatives are computed using second order centered differences and accounting for uneven grids. The vertical integration extends to the surface pressure. The pressure thickness for this lowest layer equals the surface pressure minus the pressure of the lowest reported level and the velocities and humidity assigned to the layer are those of the lowest reported pressure level.

Figures 10-13 show the changes in P, E, $P-E$, mean flow moisture convergence, the advection and mass divergence contributions to mean flow moisture convergence, the surface term and transient eddy moisture convergence for the 2021-2040 winter average minus the 1979 to 2005 winter average. Over North America (Figure 10) the MCR is projected to experience an increase in winter P but, because of warming and higher evaporative demand, its southern extent is projected to see a decrease in $P-E$. Transient eddy moisture convergence is projected to decrease across the MCR (a consequence of weaker eddies in the lower troposphere, see Seager et al. (2014c)). Increased mean flow moisture convergence provides the wetting with both the advection and mass divergence terms important. Prior work (Seager et al. 2014c; Simpson et al. 2016) has shown that this is partly thermodynamic (the MCR region is wet in winter and rising humidity in a warmer atmosphere makes it wetter) and partly due to adjustment of the stationary wave field creating a trough offshore and southwesterly winds into the MCR.

Widespread declines of P and $P-E$ are projected for the Mediterranean (Figure 11) and are largely driven by a move towards mean flow moisture divergence and the term involving

the mass divergence being key. As also shown before (Seager et al. 2014b; Zappa et al. 2015), this is related to a move towards a ridge in the region that again is linked to an adjustment in the planetary scale stationary wave field, but of unknown origin.

For South America, southern Africa and Australia (Figures 12 and 13) the models project drying (for both P and $P-E$) for the MCR regions driven by mean flow moisture divergence. In Chile the mass divergence term contributes drying for the southern part of the MCR but moisture advection is a drying term across the MCR. For the MCRs of southern Africa and Australia it is also the advection term that drives consistent drying. In all three southern hemisphere MCRs, transient eddy moisture divergence acts reactively and diffusively to provide a wetting tendency offsetting mean flow induced drying.

To assess whether these changes arises from change in the flow or the moisture field we examined the further moisture budget decomposition in Eqs. 3 and 4 and this is shown for the southern hemisphere in Figures 14 and 15. Dynamic terms are on the left and thermodynamic terms on the right. The thermodynamic term most closely related to the "wet-get-wetter" paradigm - increasing humidity in a region of low-level mass convergence (upper right) - does provide a wetting tendency in the Chile and southwest Australia MCRs (but less so in southwest southern Africa) but this is overwhelmed by a thermodynamic drying tendency due to increased drying by advection (lower right). There is also a dynamic drying tendency due to a shift towards increased low-level mass divergence in the MCR region (upper left). The moisture budget change is very similar in the MCRs of southern Africa and Australia: the thermodynamic mass convergence term provides a wetting tendency that is overwhelmed by i) thermodynamic drying due to increased dry advection and ii) dynamic drying due to increased low level mass divergence.

Next we investigate the causes of these thermodynamical and dynamical changes. In Figure 16 we show for the southern hemisphere the climatology of, and change in, humidity vertically-integrated from the surface to 600hPa and the 850hPa winds. The southern hemisphere MCRs sit within widespread subtropical minima of the increase in vertically integrated humidity. Although not shown here, computations as in Ting et al. (2018), show that this subtropical minima is associated with a reduction in relative humidity in the lower troposphere above the boundary layer. Declining free troposphere relative humidity in the

subtropics to mid-latitude region under global warming has long been noted and is explained in terms of (i) the poleward expansion of the Hadley Cell and (ii) smaller temperature increases in the upper level regions where the air was last saturated than in the regions to which the air descends (Lorenz and DeWeaver 2007; Sherwood et al. 2010; O'Gorman and Muller 2010; Wright et al. 2010; Lau and Kim 2015).

Within these subtropical regions, the humidity increase is locally minimized in the MCRs. The wind changes show a clear trend to easterlies north of $40°S$ (east Pacific) and $35°S$ (Indian Ocean) and towards westerlies to the south. Comparing to the climatological state (Figure 15, top panel), these changes represent a poleward expansion of the Hadley Cell and trade winds and a poleward shift and intensification of the extratropical westerlies. Westerly winds impinging on the coast create convergence because of topography and increased surface friction. Hence, in the region of easterly wind change, there is a shift towards low level mass divergence and, consequently, subsidence off the coasts of the MCRs, causing a reduction in specific humidity via moisture divergence. Since this process creates a local specific humidity change minimum right at and west of the coast, the moisture advection term that combines the unchanged westerly flow with the changed humidity field is a drying term for the MCRs inland. While that advection term is a thermodynamic term it should be recognized that the separation is not clean because, as mentioned, the pattern of humidity change is influenced by the circulation change.

5. Discussion

The Koppen climate classification is based entirely on long term climatological properties of a region and pays no attention to variability of climate and uses three letters for characterization. Mediterranean-type climate are identified as being temperate (C), with a dry summer (s) and hot (a) or warm (b) summers, hence both Csa and Csb climates. Despite the absence of attention to climate dynamics, the scheme successfully identifies Mediterranean-type climate regions on five continents that do share commonalities in climate, geographical locations and planetary-scale dynamical context.

As we have shown, the MCRs also have similar climatologies of precipitation and tem-

perature variability. However the causes of variability differ across the MCRs. It might be expected that given their subtropical to mid-latitude location each MCR would be subject to variability driven from the tropics and via annular modes. However, tropically-forced variability primarily arises from the Pacific and, hence, it is not surprising that the North American west coast and Chile are the prime recipients of its induced variability. Although ENSO-induced variability is global, the other MCRs are in locations remote from the tropical Pacific and/or near nodal lines in ENSO-teleconnections (the Mediterranean, southwest Southern Africa, southwest Australia) (Garreaud and Battisti 1999). In addition, in the southern hemisphere, the winter (analyzed here) is a season of growing or decaying, but not peak, ENSO variability which limits the strength of tropical forcing of circulation variability (O'Kane et al. 2017). This is consistent with the ENSO-signal in the southern Africa and Australian MCRs remaining weak in analysis of the SST-forced model ensemble mean even though that isolates the SST-forced signal by averaging over internal variability. In all MCRs the dominant source of variability appears to be internal atmosphere variability. This is understandable given their location at the equatorward flank of mid-latitude storm tracks (Hoskins and Valdes 1990; Trenberth 1991) that allow for considerable internally-generated variability (O'Kane et al. 2017). Hence, even for the ENSO-teleconnected MCRs at the western coast of the Americas, the ocean-forced signal is weak relative to internal atmospheric variability. Of other modes of ocean-related variability, the Indian Ocean Dipole Mode does influence Australian climate but the influence is weak over the MCR in the southwest (Risbey et al. 2009). The minor role for ocean forcing means that predictability of interannual variability of winter precipitation in the MCRs will largely be small beyond the timescale of numerical weather prediction based on initial conditions.

The annular modes are one major source of internal atmosphere variability in the extratropics and given their hemispheric inclusivity might be expected to influence the MCRs. However, only in the Mediterranean is the interannual variability of winter precipitation dominated by annular mode variability, also interpretable here as the NAO. As shown in Thompson and Wallace (2000) (see their Figure 1), the northern and southern annular modes variability lies somewhat poleward of the MCRs and their zonal structure is such that the Mediterranean is the only MCR that is located where there is substantial annular mode

variability.

There is commonality across the MCRs, with the exception of California, in trends over the past century towards drier winters. This is quite consistent with CMIP5 model simulations and is likely a consequence of human-driven climate change (Polade et al. 2017; Delworth and Zeng 2014). The CMIP5 models project continuation of the historical trends. The mechanisms for this can be discussed in terms of three commonly used concepts of GHG-driven hydroclimate change, and one less commonly used.

a. "Wet get wetter, dry get drier"

The expectation is that as the atmosphere warms and can hold more water, those wet areas where moisture converges will become wetter as the atmosphere converges more moisture and vice versa for dry areas of moisture divergence (Chou and Neelin 2004; Held and Soden 2006). Since in winter, MCRs are regions of moisture convergence and wet, if this mechanism was dominant we would expect the MCRs to get wetter in winter. The moisture budget analyses do show that this thermodynamics term creates a wetting tendency. However it is overwhelmed by other drying terms in all MCRs other than the North American west coast and hence "wet-get-wetter" is not a good guide for hydroclimate change in MCRs.

b. Expansion of the Hadley Cell and tropics

Lu et al. (2007) noted that global warming causes the Hadley Cell to expand as thermal stratification in the subtropics increases and moves the latitude at which the zonal flow becomes baroclinically unstable poleward. This would be expected to move the subtropical dry zones, which are under the descending branch of the winter hemisphere Hadley Cell, poleward, encroaching, at the west coast of continents, into the MCRs (see Grise et al. (2019) for a recent review of the character and causes of recent tropical expansion). The analysis shows that Hadley Cell expansion in the southern hemisphere (Feitas et al. 2017) is indeed a good way to think of the ongoing and model projected increase in aridity within the MCRs. The low level wind changes clearly show a poleward migration of the subtropical high pressure zones under the descending branch of the Hadley Cell and there is a zonal band

of decreasing precipitation at this latitude. The Hadley Cell is by definition a zonal mean phenomenon although the physical phenomenon of rising air in the tropics and descending air in the subtropics need not be zonally uniform and changes in the characteristics of these rising and descending regions may contribute to some zonally asymmetric changes. In contrast, in the northern hemisphere the greatly differing hydroclimate responses in California (wetting or little change) and the Mediterranean (strong drying) make explanation in terms only of Hadley Cell expansion inadequate and require an appeal to changes in zonally asymmetric stationary waves.

c. Poleward shift of the mid-latitude westerlies and storm tracks

Yin (2005) noted that global warming causes a poleward and upward shift of the storm tracks and an associated poleward movement of the jets and a move towards a high index state of the northern and southern annular modes. This change is part and parcel of the Hadley Cell expansion given the coupling between the axisymmetric tropical flow, the mid-latitude eddies and the jet streams (see, for example, Schneider (2006)). Our analyses here clearly show a projected poleward movement of the southern hemisphere winter westerlies which occurs owing to both the direct effect of CO_2 increase and SST warming (Grise and Polvani 2011). Within the southern MCRs this reduces the westerlies, leading to anomalous easterly flow and divergence, subsidence, reduced humidity and precipitation. In the northern hemisphere prior work has again made clear the situation is more complex. At the location of the North American MCRs, the westerlies actually shift equatorward in the model projections (Simpson et al. 2014, 2016) but over the Mediterranean-Europe sector the westerlies do not so much shift in latitude as extend eastward into northern Europe which has the effect of placing high pressure over the MCR to the south (Woollings and Blackburn 2012; Simpson et al. 2014). Hence, viewing the drying of MCRs in terms of poleward movement of the mid-latitude circulation is also valid for the southern hemisphere but not the northern hemisphere without qualification.

d. Changes in stationary waves

Due to the large continents and high, broad, mountain chains the stationary wave field in the northern hemisphere has a larger amplitude than that in the southern hemisphere. In the southern hemisphere, changes in the stationary wave field do not need to be invoked to explain the hydroclimate change in MCRs and, instead, a more zonally symmetric view in terms of the Hadley Cell and an extratropical jet stream and storm track seems adequate. That said, intensification of drying in the MCRs does arise from local interactions between the continents and the zonal mean circulation shifts. In contrast, in the northern hemisphere, changes in the stationary waves have a powerful influence on winter hydroclimate change in the MCRs. Lengthening of the zonal scale of the stationary waves that are trapped in the subtropical-midlatitude wave guide in response to subtropical westerly strengthening (according to $k \approx (\beta/\bar{u})^{1/2}$, where k is zonal wavenumber, β is the meridional gradient of the Coriolis parameter and $\bar{u}$ is the zonal mean zonal wind, for a uniform zonal flow and waves with large meridional scale), places southerly anomalies at the North American west coast that provide a wetting tendency (Simpson et al. 2016). The contrasting strong drying of the Mediterranean is also related to a stationary wave response and local high pressure (Seager et al. 2014b; Zappa et al. 2015) south of the eastward extended North Atlantic jet although the dynamics are not fully understood yet.

6. Conclusions

We have examined climate variability and change in the Mediterranean-type climate regions on five continents. Conclusions are as follows.

- The MCRs are justifiably grouped as climate types in that they have similar seasonal cycles of precipitation, temperature and variability. They also share commonality in the geographic location with reference to planetary scale dynamics. In the winter the west coast location ensures a temperate winter climate, free of continental cold air incursions and being within, or on the equatorward flank of, extratropical stormtracks makes the winters wet. The west coast location also ensures that in summer they are under the

equatorward flowing, descending branch of the subtropical anticyclones ensuring dry and warm or hot summers. The location between arid regions equatorward and more humid regions poleward ensures sizable winter season precipitation variability in all the MCRs.

- Despite the commonalities of climatology, the sources of interannual variability of winter precipitation vary notably across MCRs. Both California and Chile have modest influence from ENSO with El Niño favoring wet winters which is explainable in terms of them being downstream in the Rossby wave propagation path that originates in the equatorial Pacific deep convection anomalies driven by ENSO SST anomalies. A strong influence of annular mode variability is restricted to the Mediterranean where it is synonymous with North Atlantic Oscillation variability. For southwest southern Africa and southwest Australia, winter precipitation variability is most clearly related to the strength of local westerlies. In all regions, SST-forced models do uncover some SST-induced variability but it is weak compared to internal atmospheric variability indicating that seasonal prediction will have at best modest skill in the MCRs.

- All MCRs except in North America (California, Pacific Northwest) have experienced notable drying over the 1901 to 2016 period which reaches statistical significance at the 5% level in many parts of the MCRs. Drying of the four MCRs outside North America is highly unlikely to have occurred by chance sampling of interannual variability. This drying is also simulated in the historical simulations of the CMIP5 multimodel ensemble. These results strongly suggest that changes in radiative forcing contributed to the drying of MCRs outside North America.

- The CMIP5 models project a continuation of past trends into the near term future with, for the coming two decade period, reductions of winter precipitation in all MCRs other than the west coast of North America. The strong Mediterranean drying and lack of North American west coast drying have been previously explained in terms of changes in stationary waves that create important zonal asymmetries in climate change. For the three southern MCRs, all share common dynamical mechanisms of drying in terms of mean circulation change. First, Hadley Cell expansion and a poleward shift

of the westerlies create easterly wind anomalies at the location of the MCRs. Since prevailing westerlies, due to friction and topography, create moisture convergence in the MCRs, the easterly shift weakens this phenomena and induces drying. Second, there is a mixed dynamic-thermodynamic drying because models project coastal minima in specific humidity change at the MCRs and that allows prevailing westerlies to increase dry advection into the MCRs inland.

The ongoing climate change and future change, if it follows the model projections, will transform and move Mediterranean-type climate regions (Rubel and Kottek 2010). At the core latitudes of the regions, aridity will increase as winters become drier and temperatures increase throughout the year. On the equatorward flanks some locations that are currently Mediterranean-type climates are likely to transition into subtropical desert or subtropical steppe. Examples of this possible transition are southern California, coastal North Africa and north-central Chile. Although it needs to be quantified, it appears plausible that encroachment of subtropical aridity might mean that southern Africa and southwest Australia lose their Mediterannean-type climate regions entirely. On the poleward flanks, Mediterranean-type climate regions on the North American west coast, Chile and Iberia will move into regions that currently have the marine, cool summer climate classification. Since the vegetation in Mediterranean-type climate regions is very closely related to the climate, it would be expected that these ongoing changes will be matched, with some delay, by ecological transformation too. These suspected changes are consistent with projected changes in the Koppen-Geiger climate classifcation done by Rubel and Kottek (2010) based on earlier climate projections and they show the southern Africa and southwest Australia MCRs to greatly shrink but not to entirely disappear. Of relevance for the west coast of North America is that, while the CMIP5 models project no drying for mid winter, they do robustly project drying (reduced $P - E$) for late winter (Gao et al. 2014; Ting et al. 2018). From the direct human point of view, water resources in these regions will become increasingly strained. Ongoing year-to-year variability, if it maintains the historical amplitude, will occur against a drying mean climate so that droughts of unprecedented severity are increasingly likely to occur while the wet winters become not so wet and offer less relief. Given the lack of, or weak, predictability of winter climate in the Mediterranean-type climate regions

this offers the likelihood of the inevitable surprises of unpredicted and unprecedented serious drought. Adaptation methods based on probability assessments are already timely in each of the Mediterranean-type climate regions to plan for increasing aridity and the transformation of climate and ecosystems.

Acknowledgments.

This work was supported by NSF awards AGS 1734760, 1602581 and 1243204. TJO was supported by the Belmont Forum/JPI-Climate project INTEGRATE (NERC NE/P006809/1). We thank Giuseppe Zappa, Adam Scaife and Rene Garreaud for useful conversations, Naomi Henderson for essential work with the CMIP5 data base, moisture budgets and model simulations and Dong-Eun Lee for performing the CAM5.3 simulations, three anonymous reviewers and James Risbey for constructive criticism. RS would like to thank the staff and faculty of the Climatic Research Unit and School of the Environmental Sciences of the University of East Anglia for their great conviviality and support during an extended stay in spring 2018 when much of this work was done, and the Lamont Doherty Earth Observatory for making the visit possible.

7. Appendix

In Figures 7 and 8 we compared the observed and CMIP5 multimodel mean trends in winter precipitation over 1901 to 2016 and argued that observed trends were consistent with those expected in response to changes in radiative forcing. In the analysis of future climate change, however, we examine differences between two decade long periods. For consistency, in Figure A1 we show the observed and CMIP5 multimodel mean change in winter precipitation for the recent historical period using 1997 to 2016 minus 1971 to 1990. For the MCRs the most recent two decade period has been drier in the eastern and western Mediterranean and over much of North Africa, Chile (other than a region south of Santiago), southwest South Africa and southwest Australia. At the North American coast the recent two decade period has been drier in Washington and Mexico but wetter in northern California and Oregon.

The CMIP5 multimodel mean has drying across much of the Mediterranean and in all the southern hemisphere MCRs though typically with lesser amplitude than observed. For these four MCRs there therefore is qualitative agreement between recent decadal timescale change and that predicted by models to occur due to changes in radiative forcing. Observed and modeled changes are also consistent in having no systematic change across the west coast of North America, the one MCR not predicted to dry in the future. As expected given this early stage in the climate system response to radiative forcing, only in some areas of the MCRs do the observed changes reach modest levels of statistical significance, while only in Chile and southwest Australia is there extensive model agreement on radiatively-forced drying across the MCR. We do not expect observed and modeled decadal timescale differences over the recent historical period to be particularly comparable given that the former will be influenced by modes of natural decadal variability and random sampling of interannual and internal atmospheric variability. Nonetheless, the limited qualitative agreement between observed and modeled differences provides evidence, additional to that provided by comparison of the 116 year long trends, that the CMIP5 model ensemble is correctly simulating the response of winter precipitation in the MCRs to radiative forcing. Analyzing the physical mechanisms of observed change over the historical period, as done for models in Section 4, is not possible given the spurious trends and discontinuities in reanalyses introduced by changes in observing systems and data coverage that effect both hydrological quantities (e.g. Trenberth et al. (2011)) and measures of circulation (e.g. Grise et al. (2019)).

REFERENCES

Allan, R. J. and M. R. Haylock, 1993: Circulation features associated with the winter rainfall decrease in southwestern Australia. *J. Climate*, **6**, 1356–1367.

Aschmann, H., 1973: Distribution and peculiarity of Mediterranean ecosystems. *Mediterranean Type Ecosystems: Origin and Structure*, F. di Castri and H. A. Mooney, Eds., Springer-Verlag, Berlin, 11–19.

753 Baich-Faig, A., et al., 2011: Mediterranean diet pyramid today. Science and cultural update.
754 *Public Health Nutrition*, **14**, 2274–2284.

755 Berberry, E. H. and C. S. Vera, 1996: Characteristics of the southern hemisphere winter
756 storm track with filtered and unfiltered data. *J. Atmos. Sci.*, **53**, 468–481.

757 Bowman, D. M. J. S., G. J. Williamson, J. T. Abatzoglou, C. A. Kolden, M. A. Cochrane,
758 and A. M. S. Smith, 2017: Human exposure and sensitivity to globally extreme wildfire
759 events. *Nature Ecol. Evol.*, **1**, 0058,doi:10.1038/s41 559–016–0058.

760 Campins, J., A. Genoves, M. A. Picornell, and A. Jansa, 2011: Climatology of Mediterranean
761 cyclones using the ERA-40 dataset. *Int. J. Climatol.*, **31**, 1596–1614.

762 Chang, E. K. M., S. Lee, and K. L. Swanson, 2002: Storm track dynamics. *J. Climate*, **15**,
763 2163–2183.

764 Chou, C. and J. D. Neelin, 2004: Mechanisms of global warming impacts on regional tropical
765 precipitation. *J. Climate*, **17**, 2688–2701.

766 Cook, B., J. E. Smerdon, R. Seager, and S. Coats, 2014: Global warming and drought in
767 the 21st Century. *Clim. Dyn.*, DOI 10.1007/s00 382–014–2075–y.

768 Cook, B. I., K. J. Anchukaitis, R. Touchan, D. M. Meko, and E. R. Cook, 2016: Spatiotem-
769 poral drought variability in the Mediterranean over the last 900 years. *J. Geophys. Res.*,
770 **121**, 2060–2074.

771 Daly, C., M. Halbleib, J. I. Smith, W. P. Gibson, M. K. Doggett, G. H. Taylor, J. Curtis,
772 and P. Pasteris, 2008: Physiographically sensitive mapping of climatological temperature
773 and precipitation across the conterminous United States. *Int. J. Climatol.*, **28**, 2031–2064.

774 Delworth, T. and F. Zeng, 2014: Regional rainfall decline in Australia attributed
775 to anthropogenic greenhouse gases and ozone levels. *Nat. Geosci.*, **7**, 583–587,
776 doi:10.1038/NGEO2201.

777 di Castri, F. and H. Mooney, 1973: *Mediterranean Type Ecosystems: Origin and Structure.*
778 Ecological Studies 7, Springer Berlin Heidelberg, 405pp.

779 Feitas, A. C. V., J. S. Frederiksen, T. J. O'Kane, and T. Ambrizzi, 2017: Simulated austral
780 winter response of the Hadley circulation and stationary Rossby wave propagation to a
781 warming climate. *Clim. Dyn.*, **49**, 521–545.

782 Flocas, H. A., I. Simmonds, J. Kouroutzoglou, K. Keay, M. Hatzaki, V. Bricolas, and D. Asi-
783 makopoulos, 2010: On cyclonic tracks over the eastern Mediterranean. *J. Climate*, **23**,
784 5243–5257.

785 Franzke, C. L. E., T. J. O'Kane, D. P. Monselesan, J. S. Risbey, and I. Horenko, 2015:
786 Systematic attribution of observed Southern Hemisphere circulation trends to external
787 forcing and internal variability. *Nonlin. Proc. Geophys.*, **22**, 513–525.

788 Gao, Y., L. R. Leung, J. Lu, Y. Liu, M. Huang, and Y. Qian, 2014: Robust spring drying
789 in the Southwestern US and seasonal migration of wet/dry patterns in a warmer climate.
790 *Geophys. Res. Lett.*, **41**, 1745–1751, DOI: 10.1002/2014GL059 562.

791 Garreaud, R. D. and D. S. Battisti, 1999: Interannual (ENSO) and interdecadal (ENSO-like)
792 variability in the southern hemisphere tropospheric circulation. *J. Climate*, **12**, 2113–2123.

793 Garreaud, R. D., et al., 2018: The 2010 - 2015 megadrought in central Chile: impacts on
794 regional hydroclimate and vegetation. *Hydrol. Earth Syst. Sci.*, **21**, 6307–6327.

795 Grise, K. M. and L. M. Polvani, 2011: The response of mid-latitude jets to increased CO_2:
796 Distinguishing the roles of sea surface temperature and direct radiative forcing. *Geophys.*
797 *Res. Lett.*, **41**, 6863–6871,doi:10.1002/2014GL061 638.

798 Grise, K. M., et al., 2019: Recent tropical expansion: Natural variability or forced response?
799 *J. Climate*, doi:10.1175/JCLI–D–18–0444.1, in press.

800 Harris, I., P. D. Jones, T. J. Osborn, and D. H. Lister, 2014: Updated high-resolution grids
801 of monthly climatic observations - the CRU TS3.10. *Int. J. Climatol.*, **34**, 623–642.

802 Held, I. M. and B. J. Soden, 2006: Robust responses of the hydrological cycle to global
803 warming. *J. Climate*, **19**, 5686–5699.

804 Hoerling, M. P., J. Eischeid, J. Perlwitz, X. Quan, T. Zhang, and P. Pegion, 2012: On the
805 increased frequency of Mediterranean drought. *J. Climate*, **25**, 2146–2161.

806 Hoskins, B. and P. J. Valdes, 1990: On the existence of storm tracks. *J. Atmos. Sci.*, **47**,
807 1854–1864.

808 Hurrell, J. W., 1995: Decadal trends in the North Atlantic Oscillation: Regional tempera-
809 tures and precipitation. *Science*, **269**, 676–679.

810 Jong, B., M. Ting, and R. Seager, 2016: El Niño's impact on California precipitation:
811 seasonality, regionality, and El Niño intensity. *Env. Res. Lett.*, **11**, doi:10.1088/1748–
812 9326/11/5/054 021.

813 Kalnay, E. et al., 1996: The NCEP/NCAR 40-year reanalysis project. *Bull. Am. Meteor.*
814 *Soc.*, **77**, 437–471.

815 Kelley, C., M. Ting, R. Seager, and Y. Kushnir., 2011: The relative contributions of radiative
816 forcing and internal climate variability to the late 20th Century winter drying of the
817 Mediterranean region. *Clim. Dyn.*, **38**, 2001–2015, doi:10.1007/s00 382–011–1221–z.

818 Kistler, R., et al., 2001: The NCEP-NCAR 50-year Reanalysis: Monthly means CD-ROM
819 and documentation. *Bull. Am. Meteor. Soc.*, **82**, 247–268.

820 Lau, K.-M. and K. Kim, 2015: Robust Hadley circulation changes and increasing global
821 dryness due to CO_2 warming from CMIP5 model projections. *Proc. Nat. Acad. Sci.*, **112**,
822 3630–3635.

823 Leemans, R. and W. P. Cramer, 1991: The IIASA database for mean monthly values of
824 temperature, precipitation, and cloudiness on a global terrestrial grid. Tech. rep., IIASA
825 Technical Report RR-91-018, Laxenburg, Austria.

826 Lionello, P., et al., 2006: Cyclones in the Mediterranean region: Climatology and effects
827 on the environment. *Mediterranean Climate Variability*, P. Lionello, P. Malanotte-Rizzoli,
828 and R. Boscolo, Eds., Elsevier, Amsterdam, Netherlands, 325–372.

Lopez-Parages, J. and B. Rodriguez-Fonseca, 2012: Multidecadal modulation of El Niño influence on the Euro-Mediterranean rainfall. *Geophys. Res. Lett.*, **39**, L02 704 doi:10.1029/2011GL050 049.

Lopez-Parages, J., B. Rodriguez-Fonseca, D. Dommenget, and C. Frauen, 2016: ENSO influences on the North Atlantic-European climate: a non-linear and non-stationary approach. *Clim. Dyn.*, **47**, 2071–2084, doi:10.1007/s00 382–015–2951–0.

Lorenz, D. J. and E. T. DeWeaver, 2007: The response of the extratropical hydrological cycle to global warming. *J. Climate*, **20**, 3470–3484.

Lu, J., G. Vecchi, and T. Reichler, 2007: Expansion of the Hadley Cell under global warming. *Geophys. Res. Lett.*, **34**, doi:10.1029/2006GL028 443.

Meneghini, B., I. Simmonds, and I. N. Smith, 2007: Association between Australian rainfall and the Southern Annular Mode. *Int. J. Climatol.*, **27**, 109–121, doi:10.1002/joc.1370.

O'Gorman, P. and C. J. Muller, 2010: How closely do changes in surface and column water vapor follow Clausius-Clapeyron scaling in climate change simulations? *Env. Res. Lett.*, **5**, doi:10.1088/1748–9326/5/2/0252 077.

O'Kane, T. J., D. P. Monselesan, and J. S. Risbey, 2017: A multiscale examination of the Pacific-South America pattern. *Mon. Wea. Rev.*, **145**, 379–402.

Philippon, N., M. Rouault, Y. Richard, and A. Favre, 1985: The influence of ENSO on winter rainfall in South Africa. *Int. J. Climatol.*, **32**, 2333–2347.

Polade, S. D., A. Gershunov, D. R. Cayan, M. D. Dettinger, and D. W. Pierce, 2017: Precipitation in a warming world: Assessing projected hydro-climate changes in California and other Mediterranean climate regions. *Scientific Reports*, **7**, 10 783, doi:10.1038/s41 598–017–11 285–y.

Polvani, L. M., D. W. Waugh, G. J. P. Correa, and S. Son, 2011: Stratospheric ozone depletion: The main driver of 20th century atmospheric circulation changes in the southern hemisphere. *J. Climate*, **24**, 795–812, doi: 10.1175/2010JCLI3772.1.

Pozo-Vasquez, D., M. J. Esteban-Parra, F. S. Rodrigo, and Y. Castro-Diez, 2001: The association between ENSO and winter atmospheric circulation and temperature in the North Atlantic region. *J. Climate*, **14**, 3408–3420.

Pozo-Vasquez, D., S. R. Gamis-Fortis, J. Tovar-Pescador, M. J. Esteban-Parra, and Y. Castro-Diez, 2005: El Niño-Southern Oscillation events and associated European winter precipitation anomalies. *Int. J. Climatol.*, **25**, 17–31.

Rayner, N., D. Parker, E. Horton, C. Folland, L. Alexander, D. Rowell, E. Kent, and A. Kaplan, 2003: Global analyses of sea surface temperature, sea ice, and night marine air temperature since the late nineteenth century. *J. Geophys. Res.*, **108**, 4407, 10.1029/2002JD002 670.

Reason, C., M. Rouault, J.-L. Melice, and D. Jagadheesha, 2002: Interannual winter rainfall variability in SW South Africa and large scale ocean-atmosphere interactions. *Meteor. Atm. Phys.*, **80**, 19–29.

Risbey, J. S., M. J. Pook, P. C. McIntosh, M. C. Wheeler, and H. H. Hendon, 2009: On the remote drivers of rainfall variability in Australia. *J. Climate*, **137**, 3233–3253.

Rodwell, M. J. and B. J. Hoskins, 1996: Monsoons and the dynamics of deserts. *Quart. J. Roy. Meteor. Soc.*, **122**, 1385–1404.

Rodwell, M. J. and B. J. Hoskins, 2001: Subtropical anticyclones and summer monsoons. *J. Climate*, **14**, 3192–3211.

Rowell, D. P., 2013: Simulating SST teleconnections to Africa: What is the state of the art? *J. Climate*, **26**, 5397–5418.

Rubel, F. and M. Kottek, 2010: Observed and projected climate shifts 1901-2100 depicted by world maps of the Koppen-Geiger climate classification. *Meteorol. Z.*, **7**, 135–141.

Scaife, A., et al., 2014: Skillful long-range predictions of European and North American winters. *Geophys. Res. Lett.*, **41**, doi10.1029/2014GL059 637.

880 Schneider, T., 2006: The general circulation of the atmosphere. *Ann. Rev. Earth Planet Sci.*,
881 **34**, 655–688.

882 Schneider, T., T. Bischoff, and H. Plotka, 2015: Physics of change in synoptic midlatitude
883 temperature variability. *J. Climate*, **28**, 2312–2331.

884 Schneider, U., A. Becker, P. Finger, A. Meyer-Christoffer, B. Rudolf, and M. Ziese, 2011:
885 GPCC full data reanalysis version 6.0 at 0.5°: monthly land surface precipitation from rain
886 gauges built on GTS-based and historic data. Tech. rep., Global Precipitation Climatology
887 Centre,doi:10.5676/DWD_GPCC/FD_M_V6_050.

888 Seager, R., N. Harnik, Y. Kushnir, W. Robinson, and J. Miller, 2003a: Mechanisms of
889 hemispherically symmetric climate variability. *J. Climate*, **16**, 2960–2978.

890 Seager, R. and N. Henderson, 2013: Diagnostic computation of moisture budgets in the
891 ERA-Interim Reanalysis with reference to analysis of CMIP-archived atmospheric model
892 data. *J. Climate*, **26**, 7876–7901.

893 Seager, R., M. Hoerling, S. Schubert, H. Wang, B. Lyon, A. Kumar, J. Nakamura, and
894 N. Henderson, 2014a: Causes and predictability of the 2011-14 California drought. Tech.
895 rep., National Oceanic and Atmospheric Administration, DTF/NIDIS Assessment Report,
896 doi:10.7289/V58K771F, 42 pp.

897 Seager, R., M. Hoerling, S. Schubert, H. Wang, B. Lyon, A. Kumar, J. Nakamura, and
898 N. Henderson, 2015: Causes of the 2011-14 California drought. *J. Climate*, **28**, 6997–7024.

899 Seager, R., H. Liu, N. Henderson, I. Simpson, C. Kelley, T. Shaw, Y. Kushnir, and M. Ting,
900 2014b: Causes of increasing aridification of the Mediterranean region in response to rising
901 greenhouse gases. *J. Climate*, **27**, 4655–4676.

902 Seager, R., R. Murtugudde, N. Naik, A. Clement, N. Gordon, and J. Miller, 2003b: Air-
903 sea interaction and the seasonal cycle of the subtropical anticyclones. *J. Climate*, **16**,
904 1948–1966.

Seager, R., N. Naik, and G. A. Vecchi, 2010: Thermodynamic and dynamic mechanisms for large-scale changes in the hydrological cycle in response to global warming. *J. Climate*, **23**, 4651–4668.

Seager, R., D. Neelin, I. Simpson, H. Liu, N. Henderson, T. Shaw, Y. Kushnir, and M. Ting, 2014c: Dynamical and thermodynamical causes of large-scale changes in the hydrological cycle over North America in response to global warming. *J. Climate*, **27**, 7921–7948.

Sherwood, S. C., W. Ingram, Y. Tsushima, M. Satoh, M. Roberts, P. Liugi Vidale, and P. A. O'Gorman, 2010: Relative humidity changes in a warmer climate. *J. Geophys. Res.*, **115**, D09 104,doi:10.1029/2009JD012 585.

Simpkins, G., 2018: Running dry. *Nature Clim. Ch.*, **8**, 369.

Simpson, I., R. Seager, T. Shaw, and M. Ting, 2015: Mediterranean summer climate and the importance of Middle East topography. *J. Climate*, **28**, 1977–1996.

Simpson, I., R. Seager, M. Ting, and T. A. Shaw, 2016: Causes of change in northern hemisphere winter meridional wind and regional hydroclimate. *Nature. Clim. Ch.*, **6**, 65–70,doi:10.1038/NCLIMATE2783.

Simpson, I., T. Shaw, and R. Seager, 2014: A diagnosis of the seasonally and longitudinally varying mid-latitude circulation response to global warming. *J. Atmos. Sci.*, **71**, 2489–2515.

Smith, I. N., P. McIntosh, T. J. Ansell, C. J. C. Reason, and K. McInnes, 2000: Southwest western Australian winter rainfall and its association with Indian Ocean climate variability. *Int. J. Climatol.*, **20**, 1913–1930.

Taylor, K. E., R. J. Stouffer, and G. A. Meehl, 2012: An overview of CMIP5 and the experiment design. *Bulletin of the American Meteorological Society*, **93**, 485–498.

Thompson, D. W. J., S. Solomon, P. J. Kushner, M. H. England, K. M. Grise, and D. J. Karoly, 2011: Signatures of the Antarctic ozone hole in southern hemisphere surface climate change. *Nat. Geo.*, **4**, 741–749.

931 Thompson, D. W. J. and J. M. Wallace, 2000: Annular modes in the extratropical circulation:
932 Part I: Month-to-month variability. *J. Climate*, **13**, 1000–1016.

933 Ting, M., R. Seager, C. Li, H. Liu, and N. Henderson, 2018: Mechanisms of future spring
934 drying in the southwestern United States in CMIP5 models. *J. Climate*, **31**, 4265–4279.

935 Trenberth, K., 1991: Storm tracks in the Southern Hemisphere. *J. Atmos. Sci.*, **48**, 2159–
936 2178.

937 Trenberth, K., G. W. Branstator, D. Karoly, A. Kumar, N. Lau, and C. Ropelewski, 1998:
938 Progress during TOGA in understanding and modeling global teleconnections associated
939 with tropical sea surface temperature. *J. Geophys. Res.*, **103**, 14 291–14 324.

940 Trenberth, K., J. T. Fasullo, and J. Mackaro, 2011: Atmospheric moisture transport from
941 ocean to land and global energy flows in Reanalyses. *J. Climate*, **24**, 4907–4924.

942 Trigo, I. F., T. D. Davies, and G. R. Bigg, 1999: Objective climatology of cyclones in the
943 Mediterranean region. *J. Climate*, **12**, 1685–1696.

944 Williams, A. P., et al., 2015: Correlations between components of the water balance and
945 burned area reveal new insights for predicting forest-fire area in the southwest United
946 States. *Int. J. Wildland Fire*, **24**, 14–26.

947 Wolski, P., 2018: How severe is Cape Town's "Day Zero" drought? *Significance*, **15.2**, 24–27.

948 Woollings, T. and M. Blackburn, 2012: The North Atlantic jet stream under climate change
949 and its relation to the NAO and EA patterns. *J. Climate*, **25**, 886–902.

950 Wright, J. S., A. S. Sobel, and J. Galewsky, 2010: Diagnosis of zonal mean relative humidity
951 changes in a warmer climate. *J. Climate*, **23**, 4556–4569.

952 Yin, J. H., 2005: A consistent poleward shift of the storm tracks in simulations of 21st
953 century climate. *Geophys. Res. Lett.*, **32**, L18 701, doi:10/1029/2005GL023 684.

954 Zappa, G., B. J. Hoskins, and T. G. Shepherd, 2015: The dependence of wintertime Mediter-
955 ranean precipitation on the atmospheric circulation response to climate change. *Env. Res.*
956 *Lett.*, **10**, doi:10.1088/1748–9326/10/12/129 501.

List of Tables

Institute	Model	Resolution (lon x lat), level	Ensemble size	
			20thC	rcp85
Beijing Climate Center (BCC)	1. bcc-csm1-1	T42, L26	1	1
	2. bcc-csm1-1-m	T106, L26	1	1
College of Global Change and Earth System Science, Beijing Normal University (BNU)	3. BNU-ESM	T42, L26	1	1
Canadian Centre for Climate Modeling and Analysis (CCCma)	4. CanESM2	T63 (1.875°x1.875°), L35	1	1
National Center for Atmospheric Research (NCAR)	5. CCSM4	288x200 (1.25°x0.9°), L26	1	1
Centro Euro-Mediterraneo per I Cambiamenti Climatici (CMCC)	6. CMCC-CM	T159, L31	1	1
Centre National de Recherches Meteorologiques / Centre Europeen de Recherche et Formation Avancees en Calcul Scientifique (CNRM-CERFACS)	7. CNRM-CM5	T127(1.4°x1.4°), L31	1	1
Commonwealth Scientific and Industrial Research Organisation in collaboration with the Queensland Climate Change Centre of Excellence (CSIRO-QCCCE)	8. CSIRO-Mk3-6-0	T63(1.875°x1.875°), L18	1	1
Institute of Atmospheric Physics, Chinese Academy of Sciences and Tsinghua University (LASG-CESS)	9. FGOALS-g2	128x60, L26	2	1
Geophysical Fluid Dynamics Laboratory (NOAA GFDL)	10. GFDL-CM3	C48 (2.5°x2.0°), L48	5	1
	11. GFDL-ESM2G	144x90 (2.5°x2.0°), L24	1	1
	12. GFDL-ESM2M	144x90 (2.5°x2.0°), L24	1	1
NASA Goddard Institute for Space Studies (NASA GISS)	13. GISS-E2-H	2.5°x2°, L40	1	1
	14. GISS-E2-R	2.5°x2°, L40	1	1
Institut Pierre-Simon Laplace (IPSL)	15. IPSL-CM5A-LR	3.75°x1.875°, L39	6	3
	16. IPSL-CM5A-MR	2.5°x1.25°, L39	2	1
	17. IPSL-CM5B-LR	96x96 (3.75°x1.875°) , L39	1	1
Atmosphere and Ocean Research Institute (The University of Tokyo), National Institute for Environmental Studies, and Japan Agency for Marine-Earth Science and Technology (AORI/NIES/JAMSTEC)	18. MIROC5	T85, L40	5	1
	19. MIROC-ESM	T42, L80	3	1
	20. MIROC-ESM-CHEM	T42, L80	1	1
Meteorological Research Institute (MRI)	21. MRI-CGCM3	TL159 (1.125°x1.125°), L48	1	1
Norwegian Climate Centre (NCC)	22. NorESM1-M	144x96 (2.5°x1.875°), L26	3	1

TABLE 1. CMIP5 models used in this study with information on host institute, resolutions (L refers to number of vertical levels, T to triangular truncation and C to cubed sphere) and ensemble sizes.

List of Figures

9 The number of models (out of 22) that agree on the sign of change of winter precipitation and also agree with the sign of change of the model ensemble mean. Green colors indicate agreement is for wetting and brown colors for drying. Stippling marks where three quarters or more of models agree. 50

10 CMIP5 multimodel mean-projected changes in the winter moisture budget in the North America region for the near term future (2021-2040) minus the recent past (1979-2005) using emissions scenario RCP85 and the historical simulations. Shown are change in a) P, b) E, c) $P - E$, d) the mean flow moisture convergence, e) the component of d) related to mass divergence, f) the component of d) related to moisture advection, g) the surface term and h) the transient eddy moisture convergence. Units are mm/day. 51

11 Same as Figure 10 but for the Mediterranean region. 52

12 Same as Figure 10 but for the South America region. 53

13 Same as Figure 10 but for the Africa and Australia region. 54

14 Further breakdown of the CMIP5 multimodel mean-projected changes in the winter moisture budget here for the South America region. Changes in the mean flow moisture convergence are broken down into components due to circulation changes (dynamic component, left) and moisture changes (thermodynamic component, right) and related to mass divergence (upper) and moisture advection (lower). Units are mm/day. 55

15 Same as Figure 14 but for the Africa and Australia region. 56

16 The climatological specific humidity integrated from surface to 600hPa (color) and 850hPa winds (vectors) (top) and the 2021-2040 minus 1979-2005 change in these (bottom) for the southern hemisphere. Units are kg/m^2 and m/s. 57

17 Figure A1. The CRU TS3.25 observed (top) and CMIP5 multimodel mean (bottom) difference in winter precipitation for 1997-2016 minus 1971-1990. In the upper panel for the observed data the tick marks show where the differences between the means of the two-decade periods is significant at the 10% level according to a two-sided t-test. In the lower panel for the models the tick marks show where 3/4 of the models agree on the sign of the change and agree with the sign of the multimodel mean change. Units are mm/day. 58

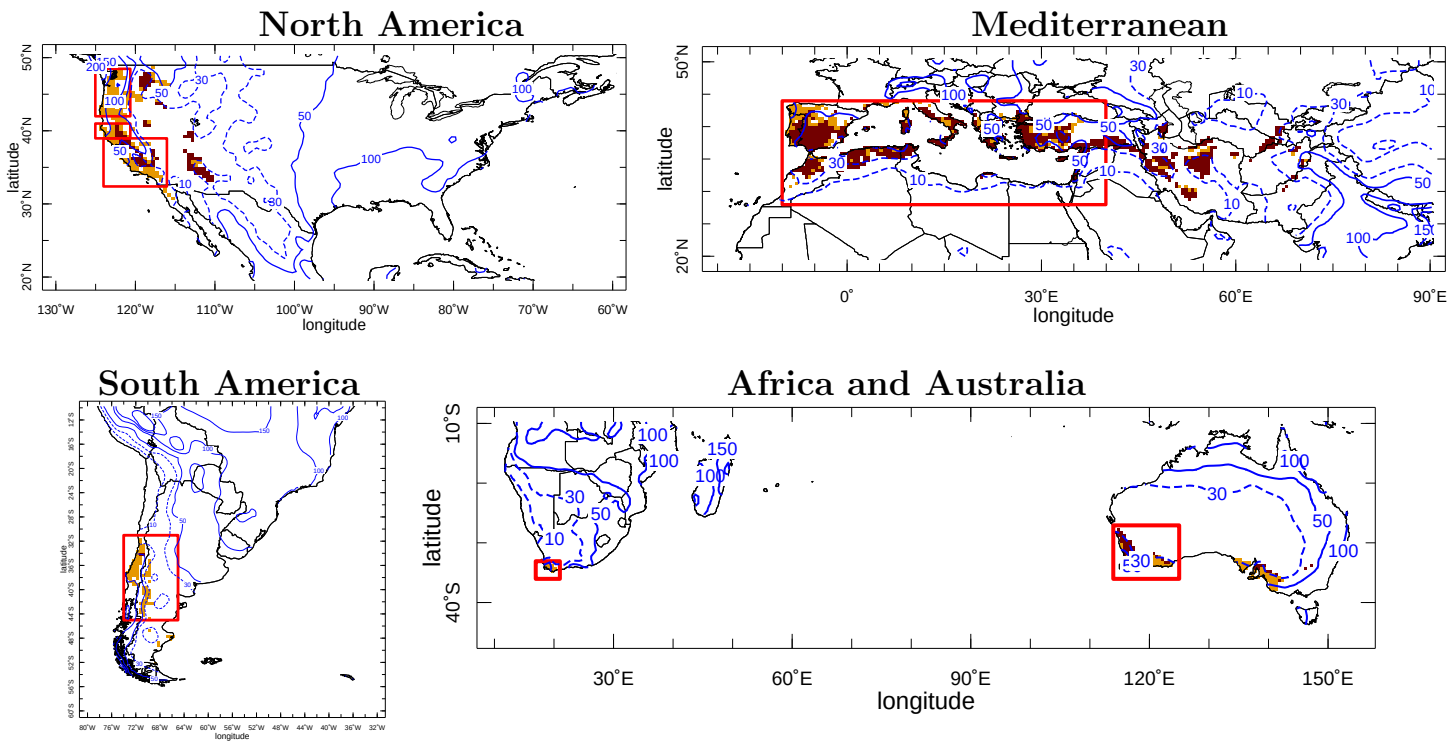

FIG. 1. Location of Mediterranean-type climate regions (color). Burgundy color shows the hot summer type of Mediterranean climate (Csa in the Koppen classification) and orange shows the warm summer type of Mediterranean climate (Csb in the Koppen classification). Also shown as contours is the annual mean precipitation over land from CRU TS v3.25 in mm/month, with dotted contours indicating values less than 50mm/month. Area averages are taken over the Mediterranean climate areas shown by the colored areas within the red boxes.

Seasonal Observed Climatology

Precipitation (color)

200 mb V'^2 (contours) SLP (contours)

NH Winter, SH Summer

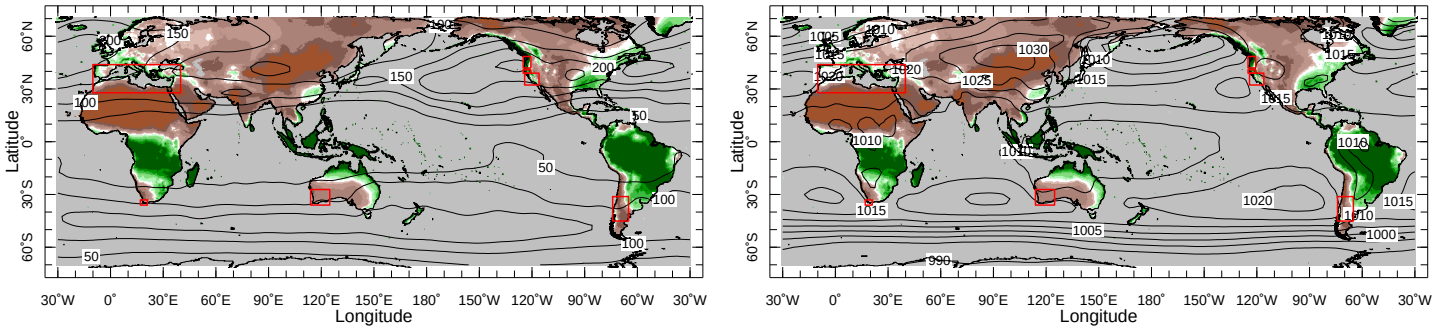

NH Summer, SH Winter

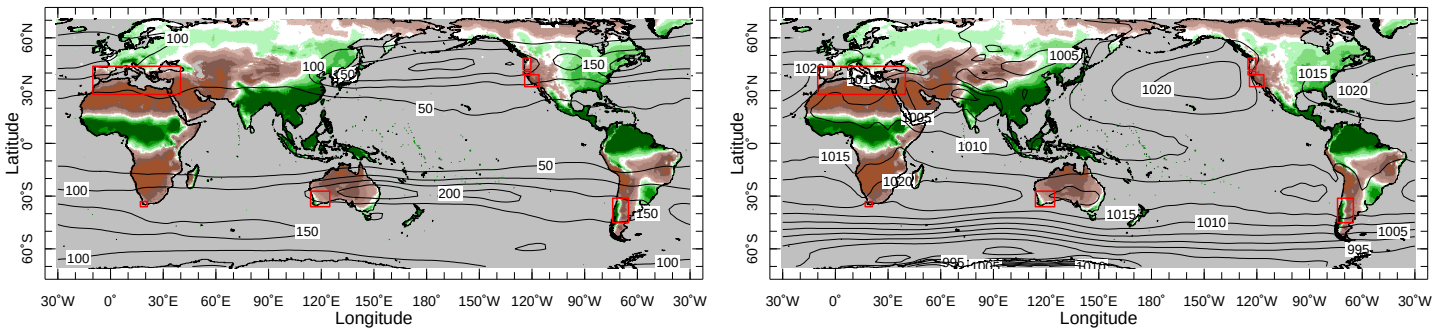

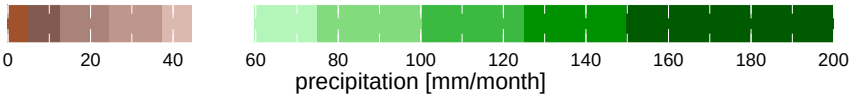

FIG. 2. Precipitation over land (mm/month) for northern hemisphere winter/southern hemisphere summer (top) and northern hemisphere summer/southern hemisphere winter (bottom). Also shown are sub-monthly 200hPa meridional velocity variance (m^2/s^{-2}), a measure of the mid-latitude storm track (left) and sea level pressure (hPa, right).

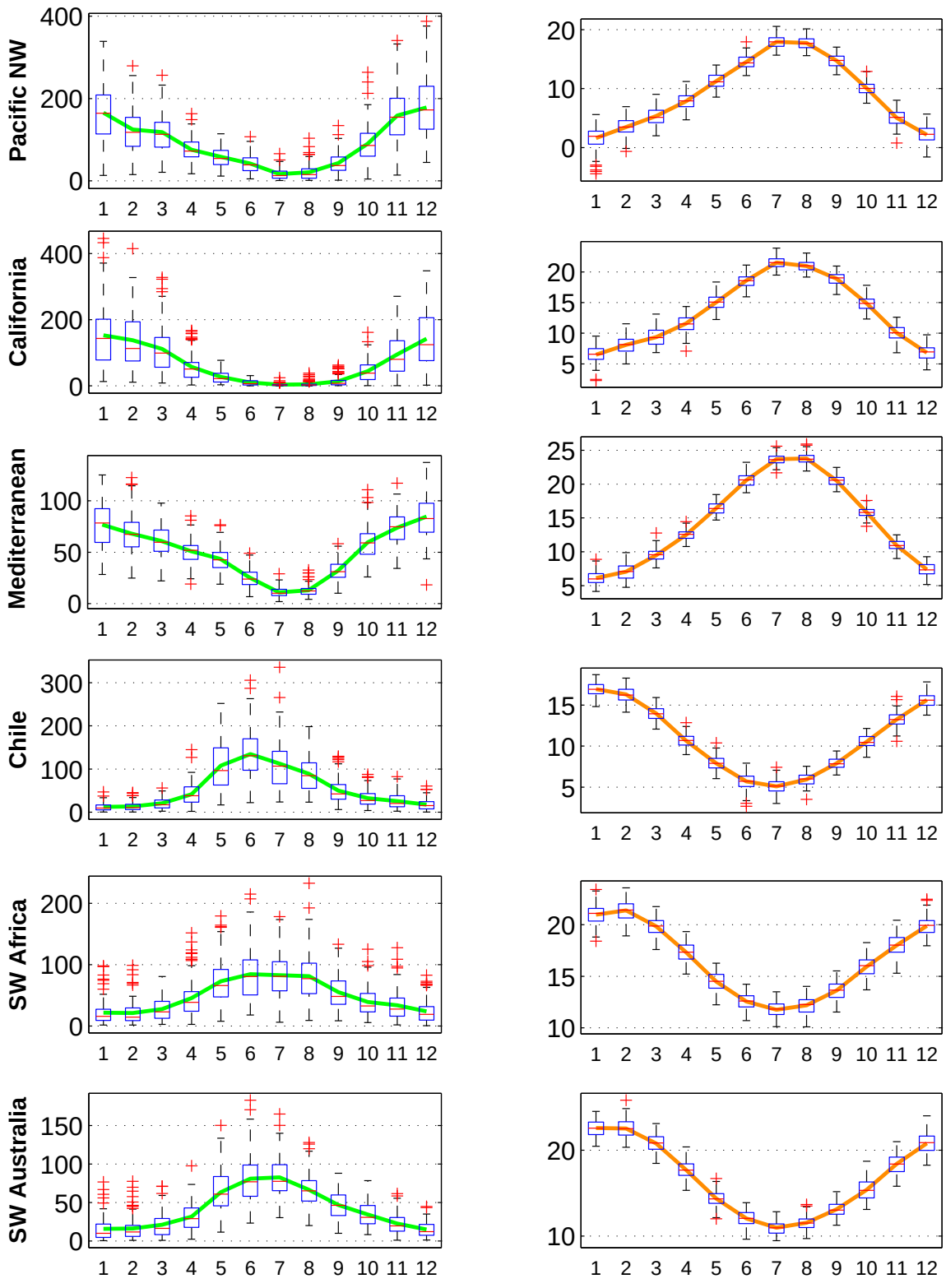

FIG. 3. The climatological seasonal cycles and variability of precipitation (left) and temperature (right) in the Mediterranean climate regions. The means are shown by the lines and the box and whiskers plotted for each month show the median (line across box), 25th and 75th percentiles (edges of box), range and outliers (beyond 2.7 σ for a normal distribution) as red crosses. Units are mm/month and deg C.

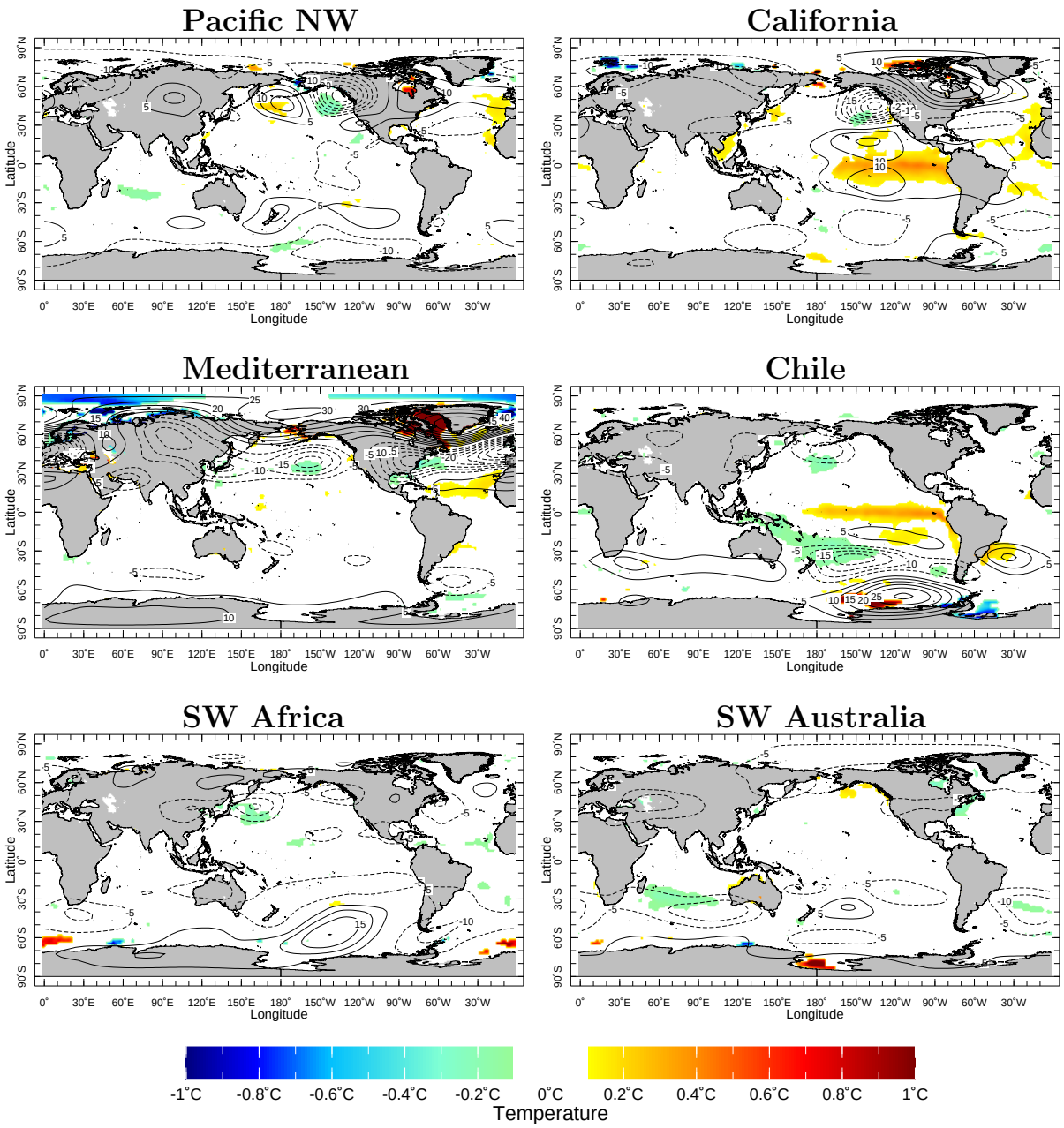

FIG. 4. The regression of SST (colors, deg C) and 200hPa geopotential heights (contours, m) onto the winter precipitation time series of each Mediterranean-type climate region, after detrending. The SSTs are plotted only where the relation is statistically significant at the 5% level.

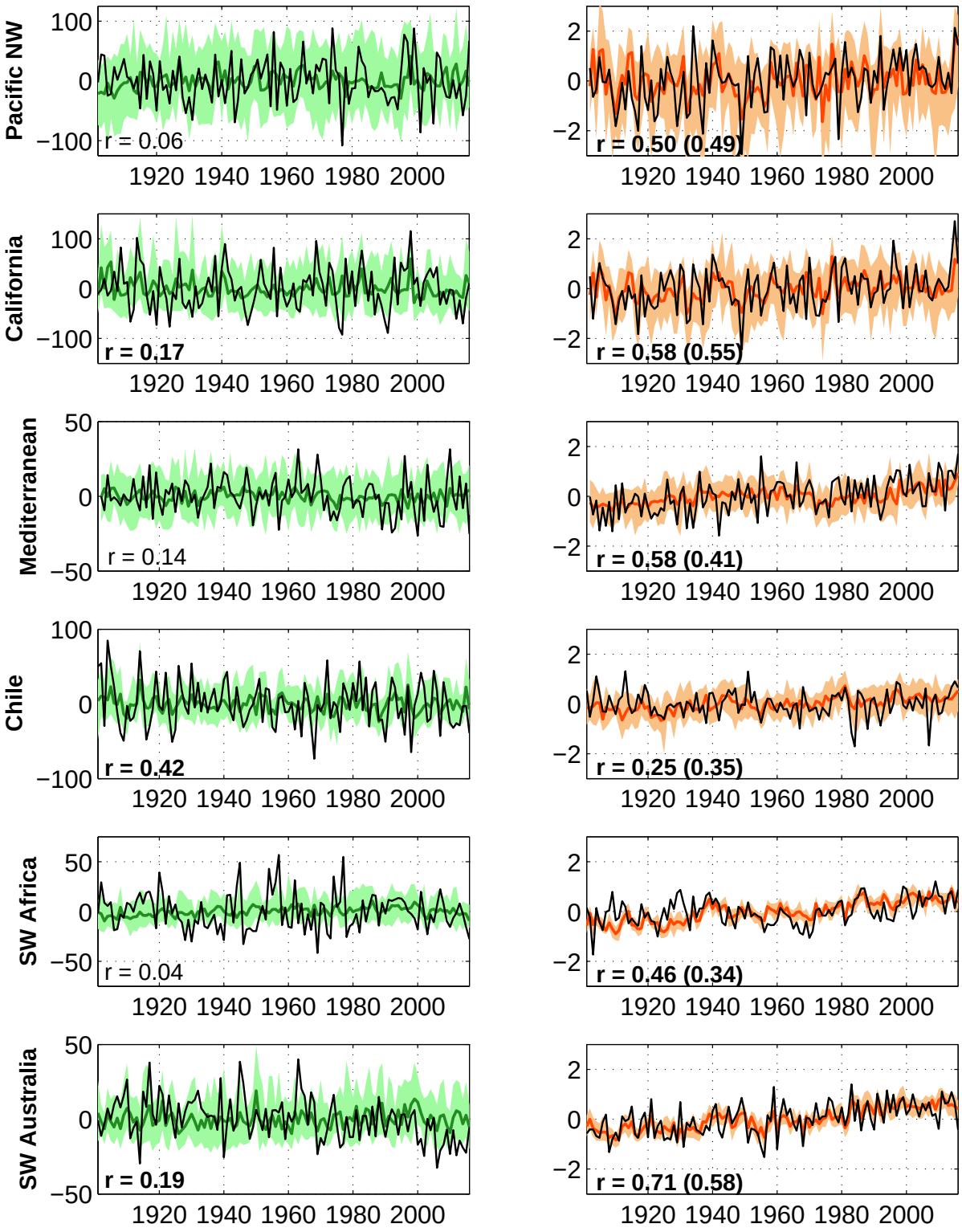

FIG. 5. The time histories of winter precipitation (left) and temperature (right) in the Mediterranean-type climate regions for observations (black line) and the SST-forced CAM5.3 model ensemble mean precipitation (green, left) and temperature (red, right) together with ensemble spread (shading). At bottom left the numbers are the correlation coefficient between the observations and the ensemble mean and, for temperature the values in parentheses are for linearly detrended data, and bold values are significant at the 5% level according to a two-sided t-test. Units are mm/month and deg C.

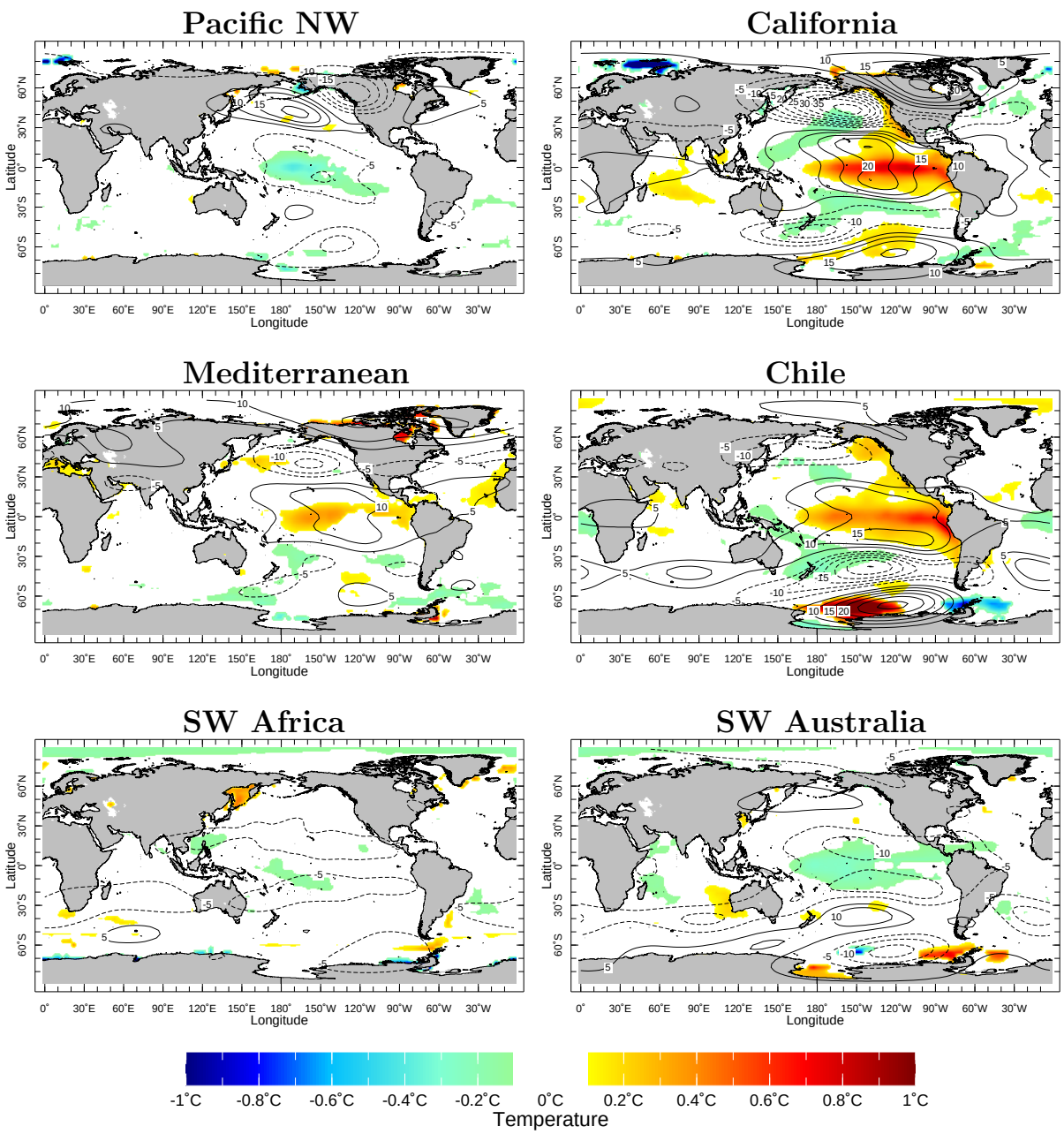

FIG. 6. As in Figure 4 but for the ensemble mean of the SST-forced simulations with the CAM5.3 model isolating the ocean-driven component of modeled winter precipitation variability in the Mediterranean-type climate regions.

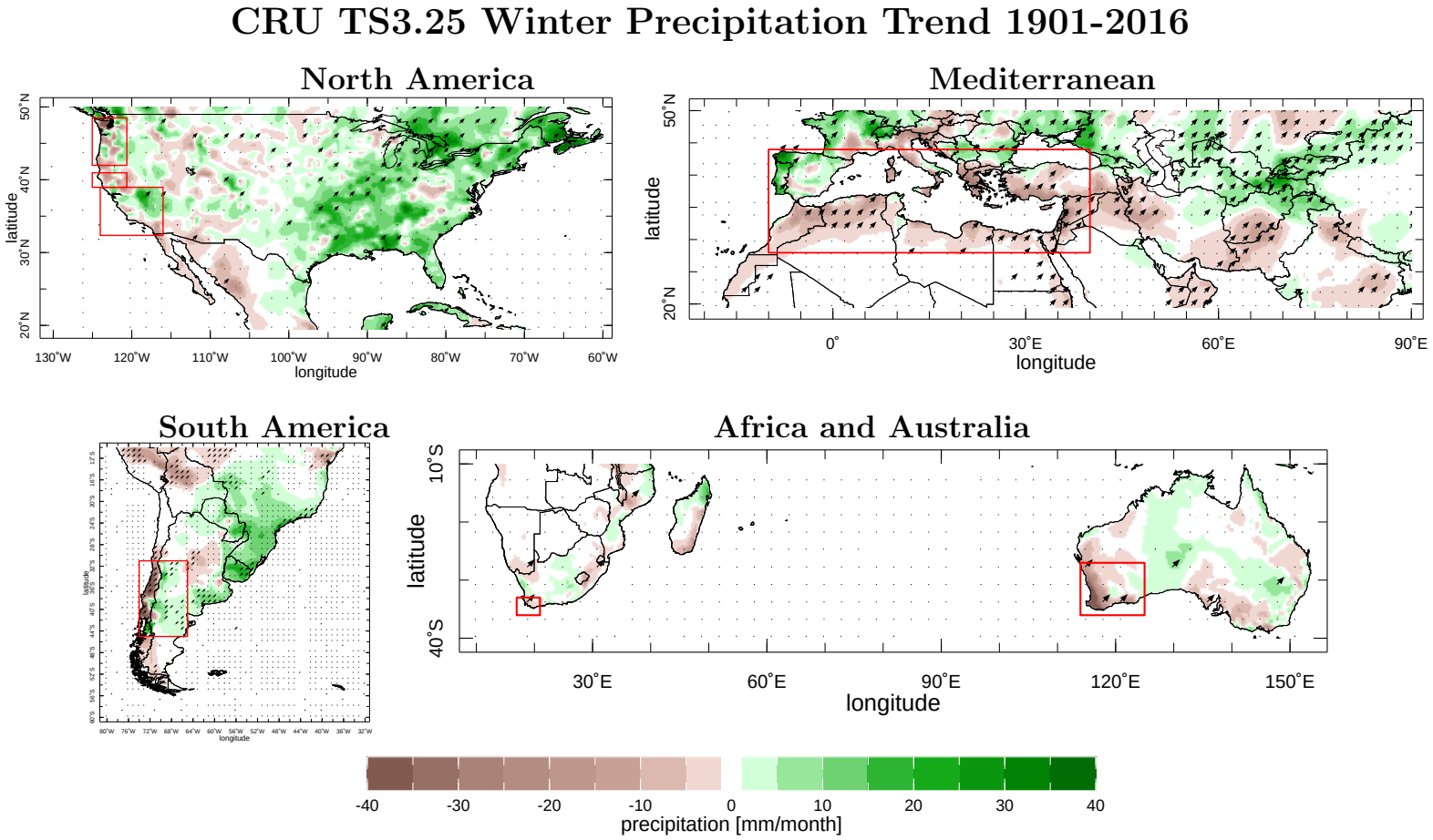

FIG. 7. The linear trend over 1901 to 2016 of winter precipitation showing the Mediterranean climate regions. Stippled locations mark significance of the trend at the 5% level according to a two-sided t-test. Units are mm/month change over the 116 years.

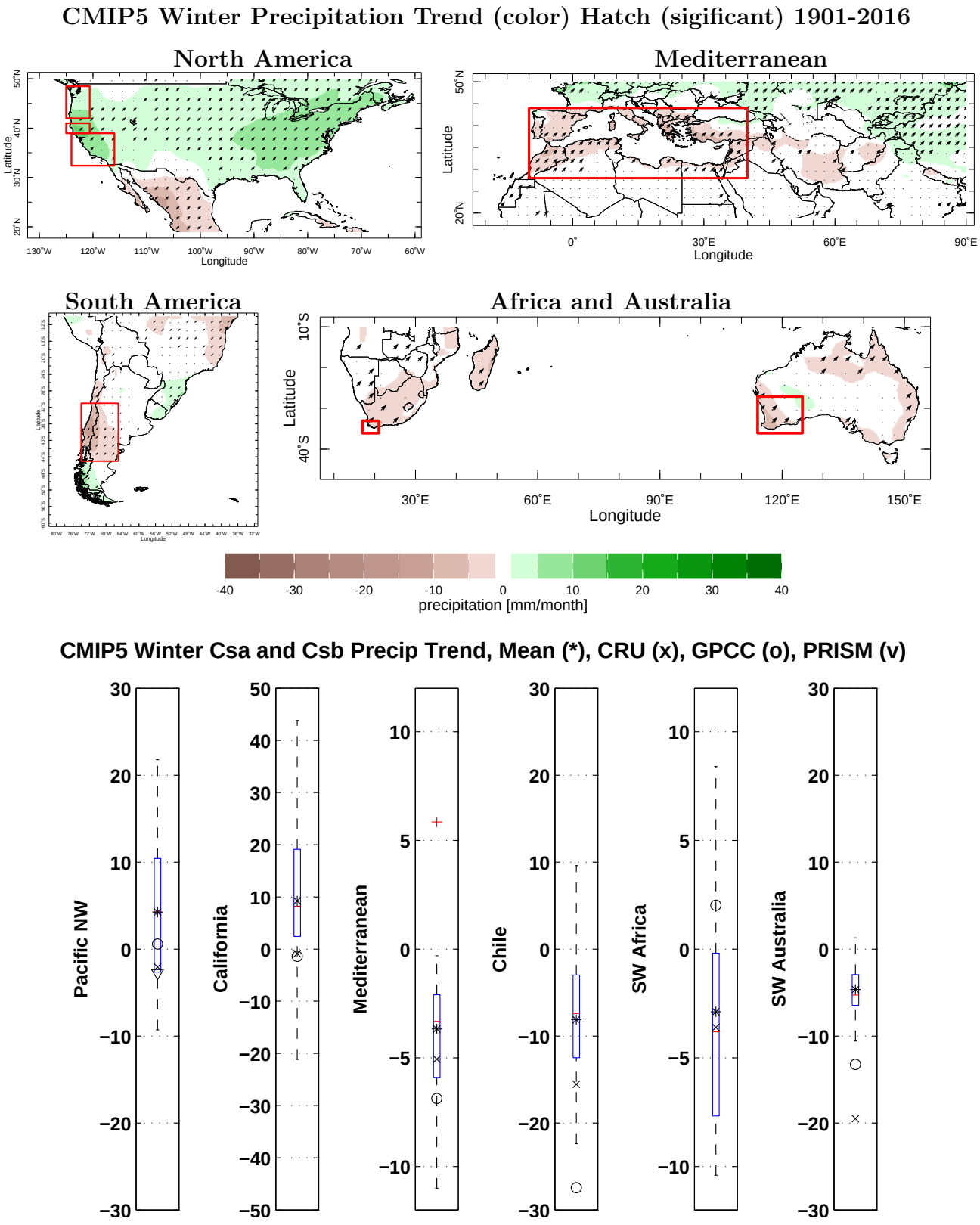

FIG. 8. Upper panel: same as Figure 7 but for the multimodel mean of the CMIP5 models using the historical simulation for 1901 to 2005 and the RCP85 emissions scenario for 2006 to 2016. Stippled locations mark where three quarters of the models agree on sign of change and with sign of change of the ensemble mean. In the lower panel the distribution of modeled trends are shown by box and whisker plots: the median, 25th and 75th percentiles are shown by the horizontal line across the box and its limits, the range by whiskers, outliers by a red cross and the mean by a black asterisk. Also shown are the CRU, GPCC and, for California and the Pacific northwest, the PRISM trends. Units are mm/month change over 116 years.

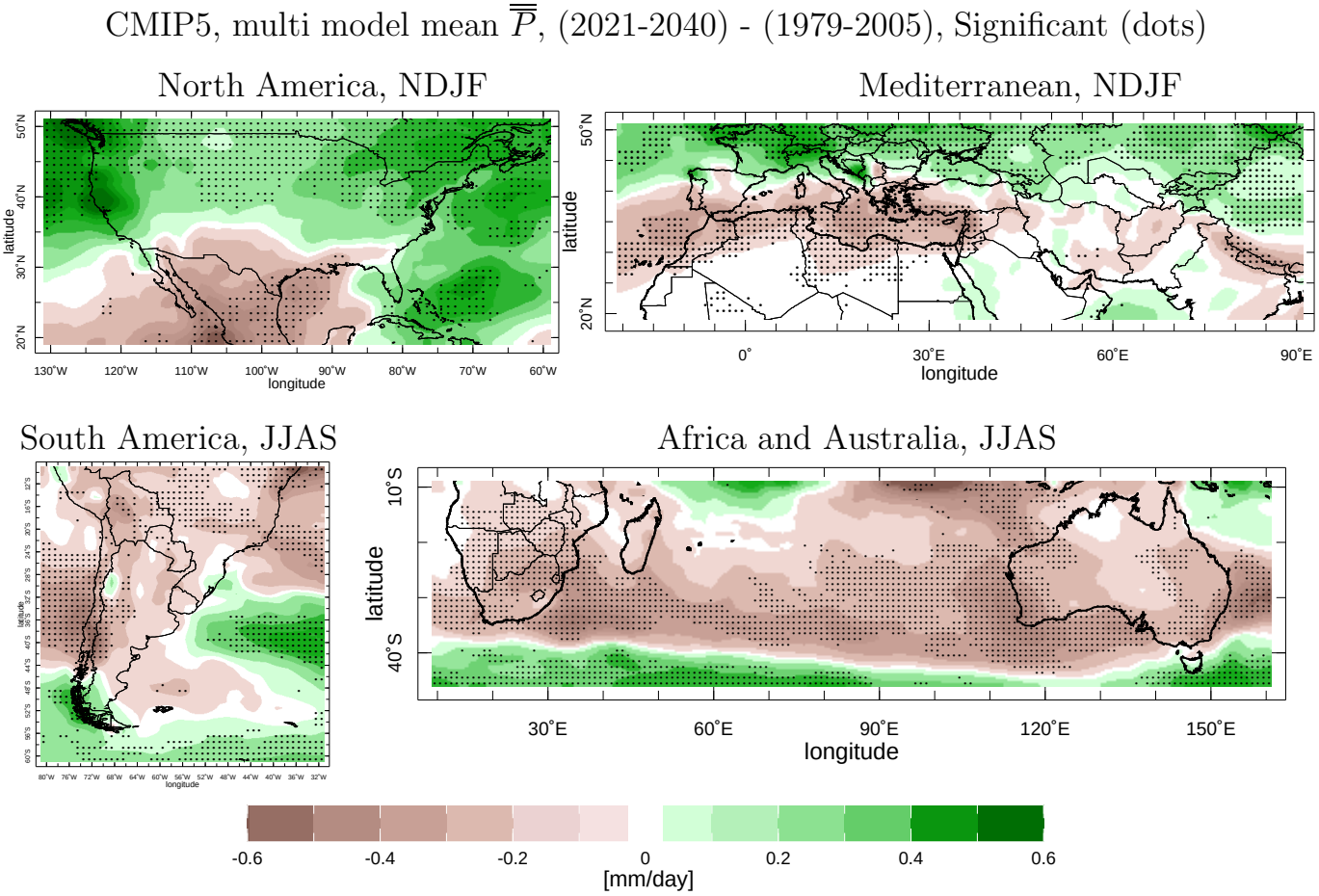

FIG. 9. The number of models (out of 22) that agree on the sign of change of winter precipitation and also agree with the sign of change of the model ensemble mean. Green colors indicate agreement is for wetting and brown colors for drying. Stippling marks where three quarters or more of models agree.

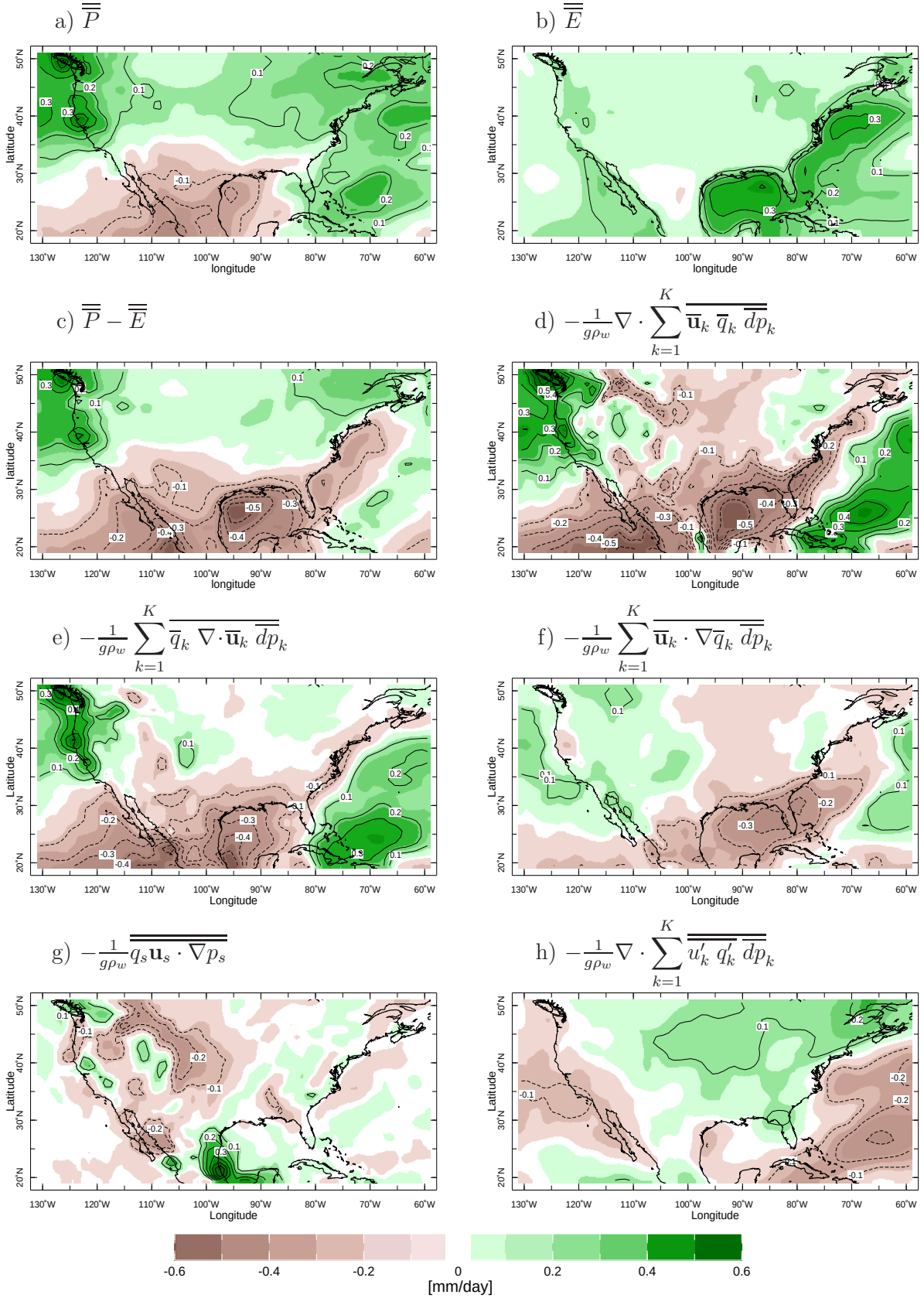

FIG. 10. CMIP5 multimodel mean-projected changes in the winter moisture budget in the North America region for the near term future (2021-2040) minus the recent past (1979-2005) using emissions scenario RCP85 and the historical simulations. Shown are change in a) P, b) E, c) $P - E$, d) the mean flow moisture convergence, e) the component of d) related to mass divergence, f) the component of d) related to moisture advection, g) the surface term and h) the transient eddy moisture convergence. Units are mm/day.

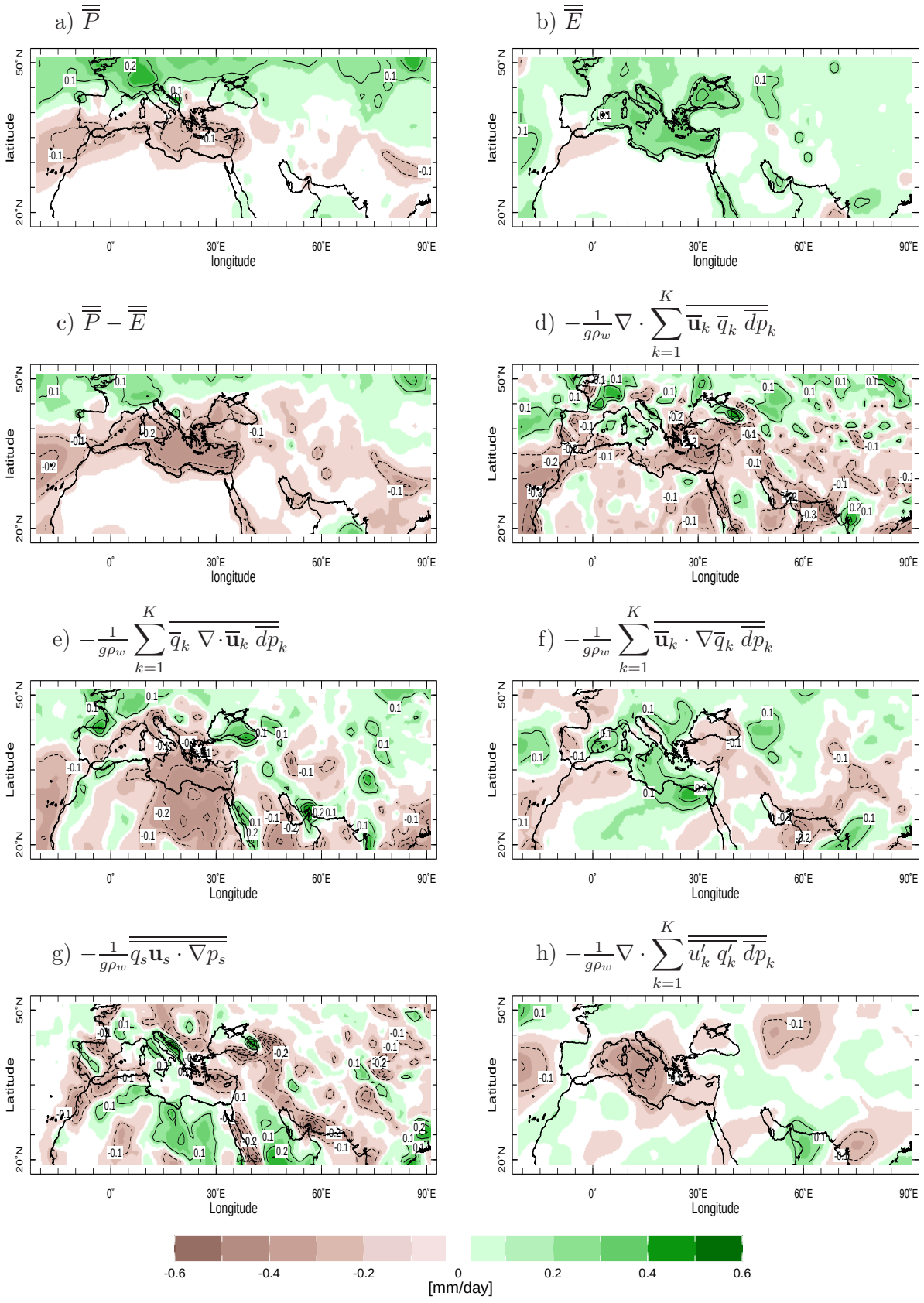

FIG. 11. Same as Figure 10 but for the Mediterranean region.

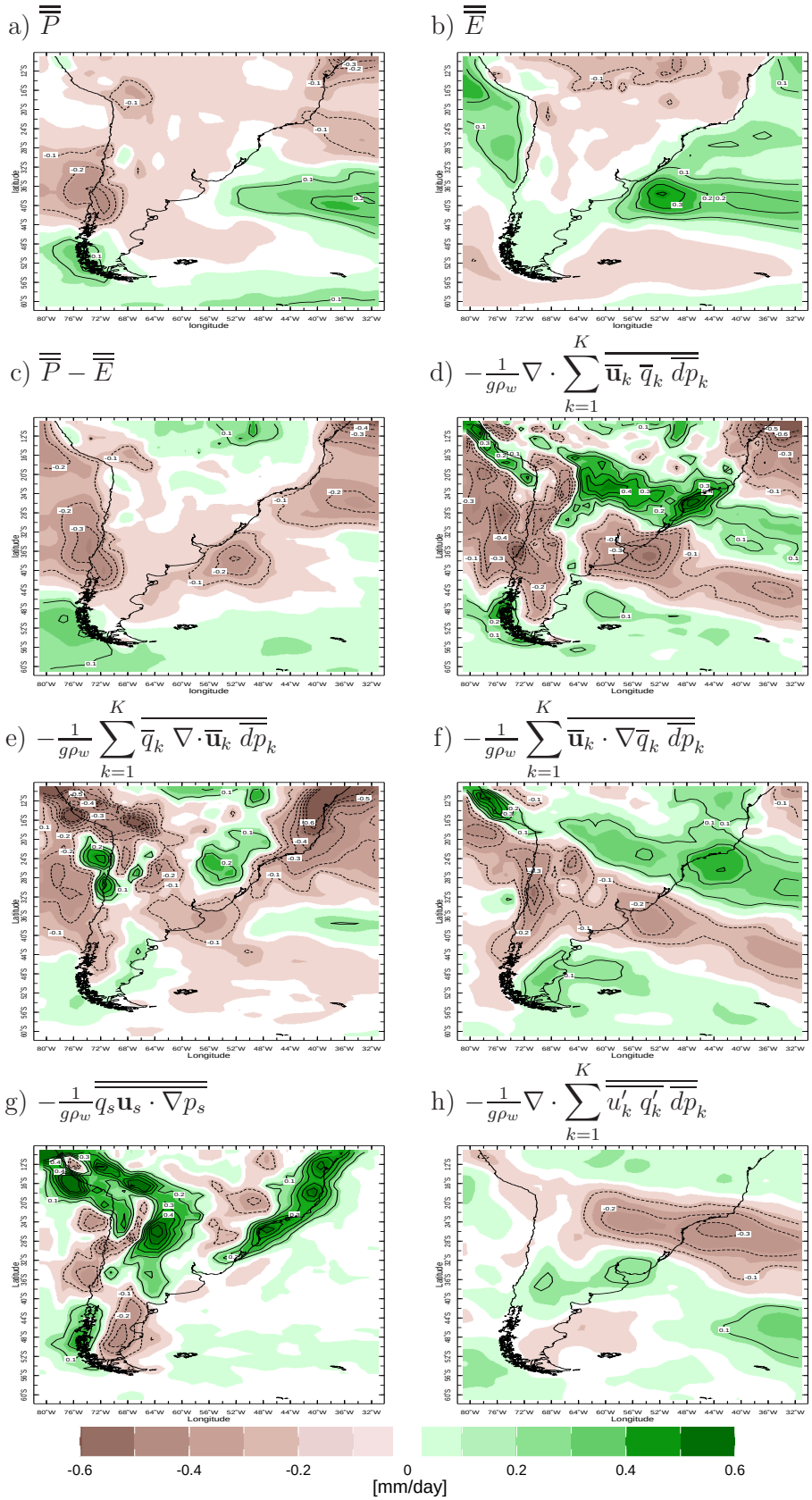

FIG. 12. Same as Figure 10 but for the South America region.

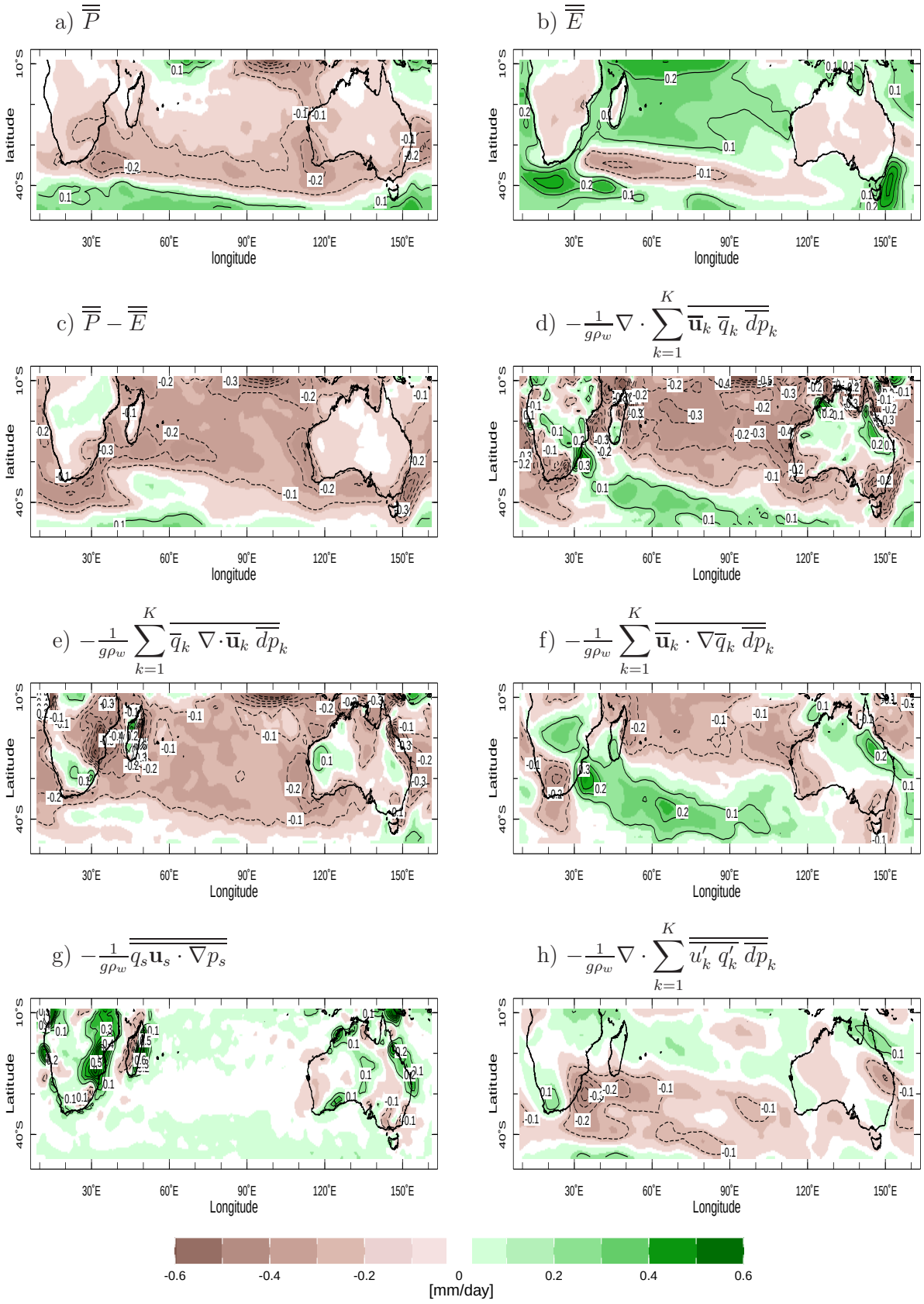

FIG. 13. Same as Figure 10 but for the Africa and Australia region.

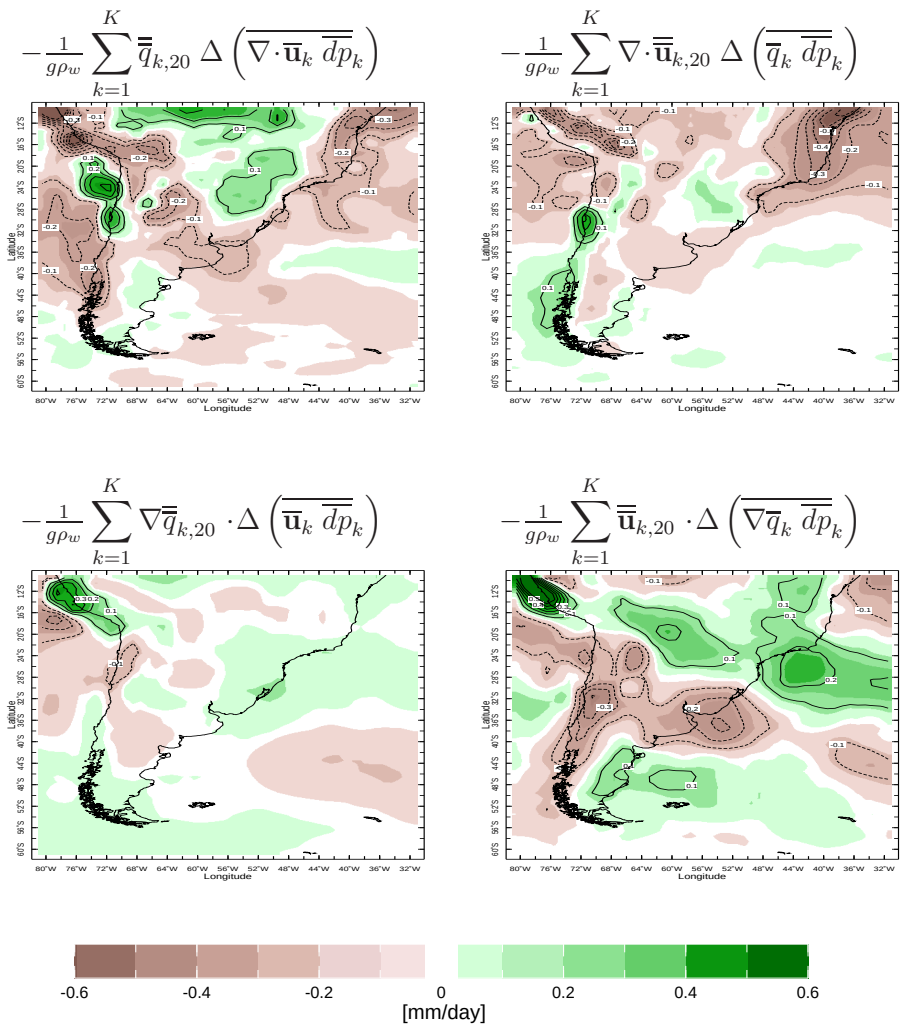

FIG. 14. Further breakdown of the CMIP5 multimodel mean-projected changes in the winter moisture budget here for the South America region. Changes in the mean flow moisture convergence are broken down into components due to circulation changes (dynamic component, left) and moisture changes (thermodynamic component, right) and related to mass divergence (upper) and moisture advection (lower). Units are mm/day.

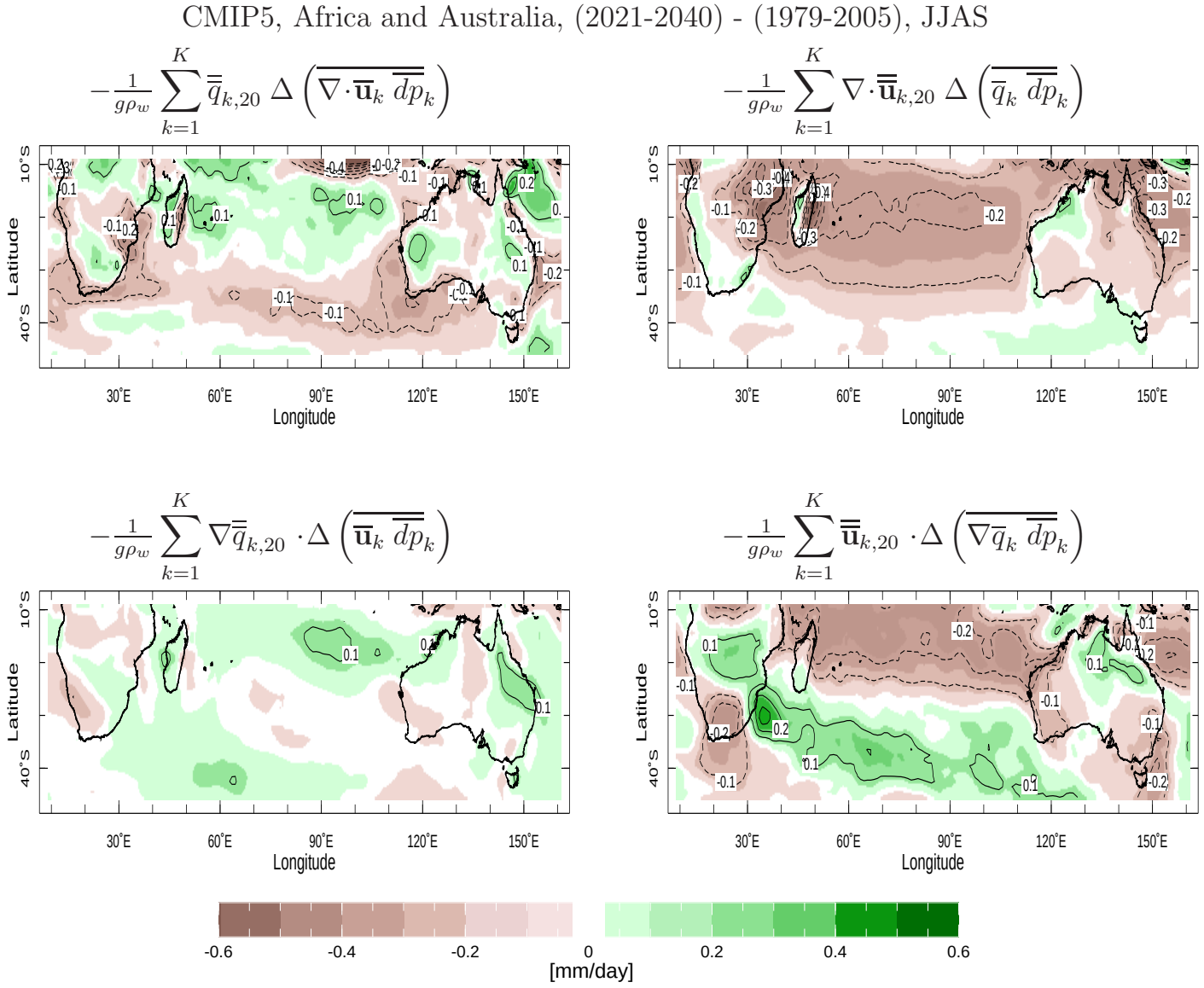

FIG. 15. Same as Figure 14 but for the Africa and Australia region.

CMIP5, (1979-2005) JJAS Climatology (color), $\frac{1}{g}\sum_{k=1}^{K} \Delta\overline{q}_k \, \overline{dp}_k$

(1979-2005) JJAS Climatology of 850hPa winds (vector, m/s)

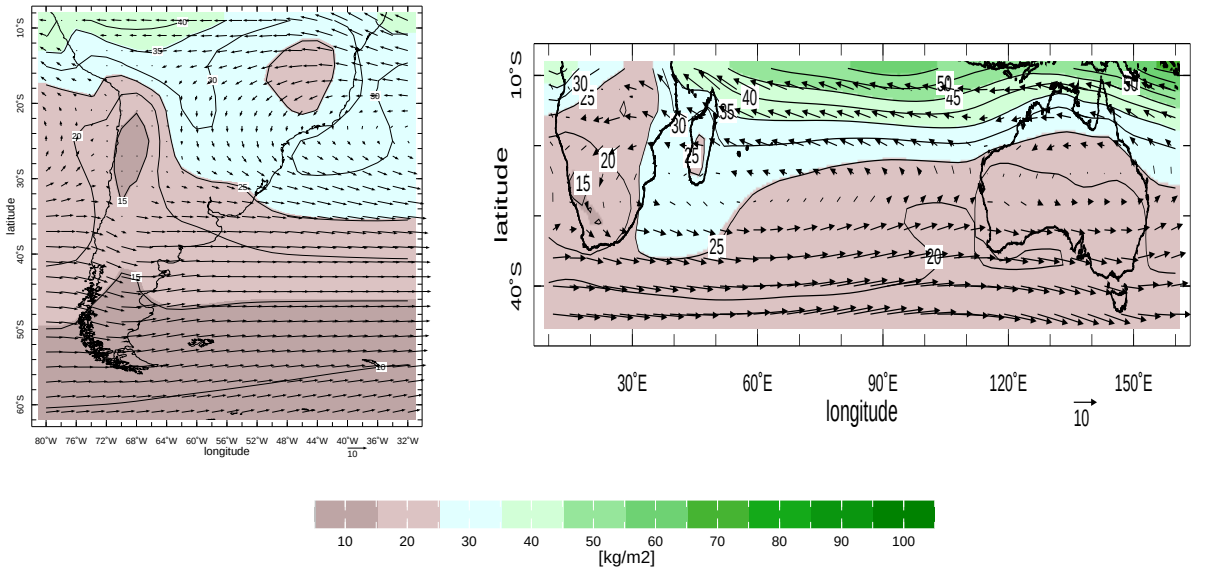

CMIP5, (2021-2040) - (1979-2005) JJAS (color), $\frac{1}{g}\sum_{k=1}^{K} \Delta\overline{q}_k \, \overline{dp}_k$

(2021-2040) - (1979-2005) JJAS of 850hPa winds (vector, m/s)

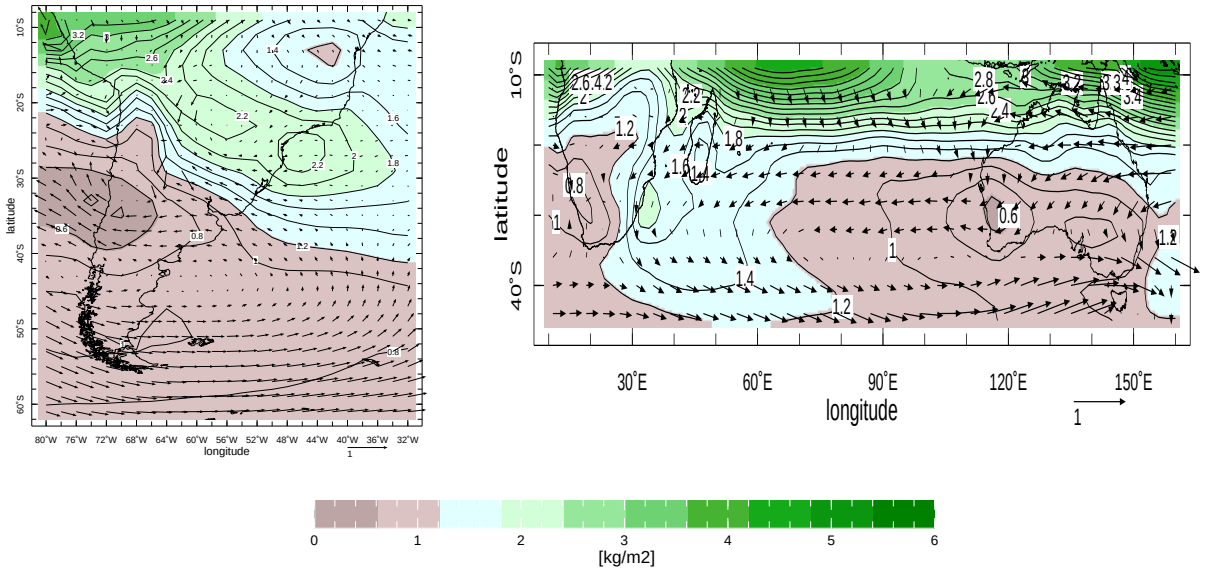

FIG. 16. The climatological specific humidity integrated from surface to 600hPa (color) and 850hPa winds (vectors) (top) and the 2021-2040 minus 1979-2005 change in these (bottom) for the southern hemisphere. Units are kg/m^2 and m/s.

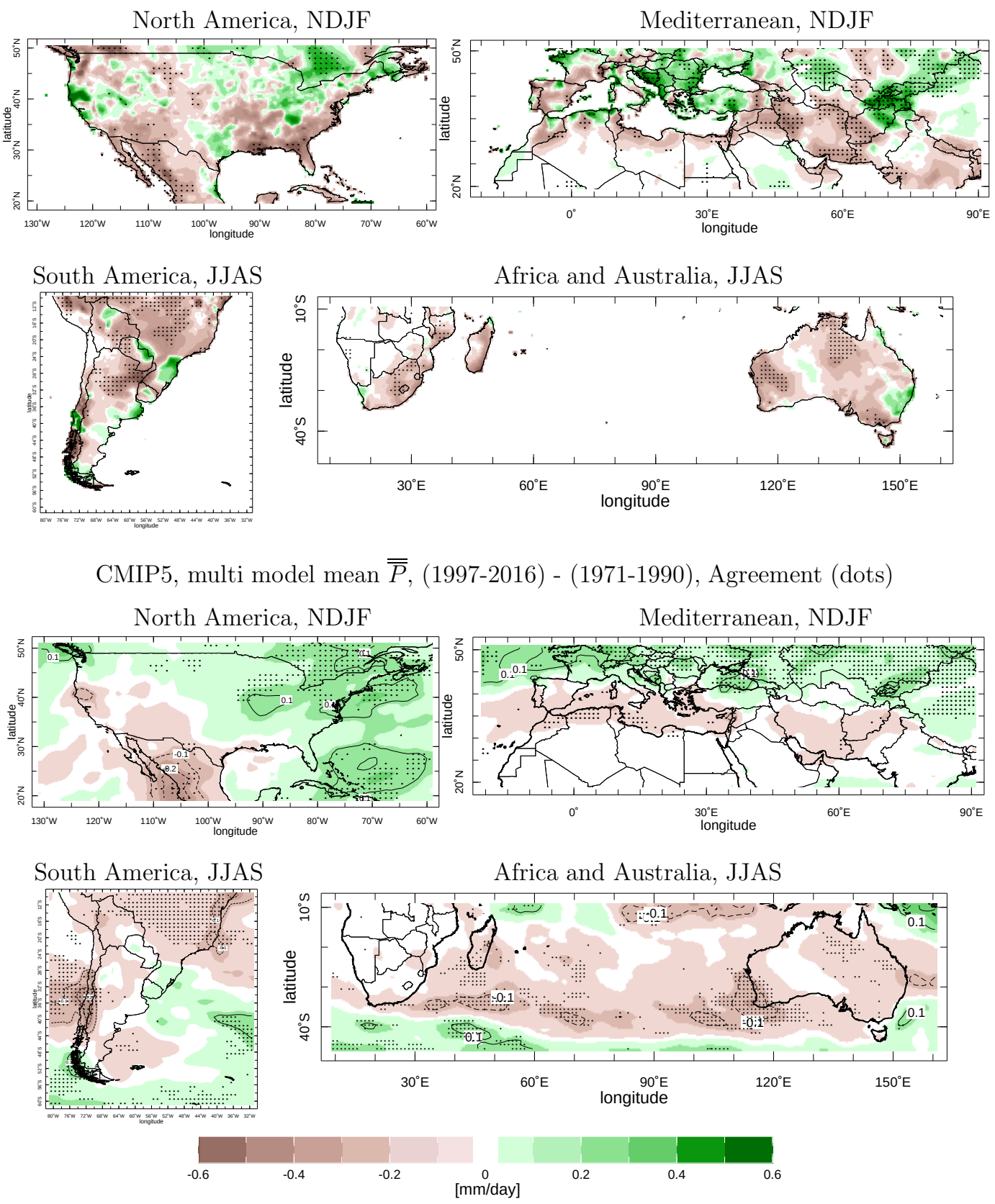

FIG. 17. Figure A1. The CRU TS3.25 observed (top) and CMIP5 multimodel mean (bottom) difference in winter precipitation for 1997-2016 minus 1971-1990. In the upper panel for the observed data the tick marks show where the differences between the means of the two-decade periods is significant at the 10% level according to a two-sided t-test. In the lower panel for the models the tick marks show where 3/4 of the models agree on the sign of the change and agree with the sign of the multimodel mean change. Units are mm/day.